(12)

(12)

ARVIN
CALSPAN CORPORATION

ADVANCED TECHNOLOGY CENTER

EXPERIMENTAL INVESTIGATIONS OF THE DEVELOPMENT OF THE MARINE AEROSOL POPULATION

B.J. Wattle, C.W. Rogers, M.C. Flanigan and R.J. Pilie'
Physical and Chemical Sciences Department

Calspan Report No. 7614-1
October 1992

Contract No. N00014-87-C-0836

Prepared for:

OFFICE OF NAVAL RESEARCH
800 NORTH QUINCY STREET
ARLINGTON, VA 22217-5000
ATTN: GG, CODE 1241

CALSPAN ADVANCED TECHNOLOGY CENTER P.O. BOX 400 BUFFALO, NY 14225

Table of Contents

Table of Contents (cont.)

List of Figures

List of Tables

Section 1

INTRODUCTION

This report describes a series of experiments designed to study the air mass directly above the ocean in an effort to better understand the development of the atmospheric aerosols which comprise marine haze. To determine the nature of the boundary layer haze, one must first characterize the composition and size distribution of the particles that comprise the haze, identify the source(s) of those particles and specify the source strength and growth rate of the resulting aerosol. Ultimately, of course, development of a model of the complete system is desired so that better forecasts of haze over the ocean can be made.

Calspan has been associated with continuing Navy programs since 1970 with participation in and management of numerous cruises for both the Office of Naval Research (ONR) and the Naval Research Laboratory (NRL). The initial programs focused on the study of fog formation which then evolved into investigations directed at characterizing the marine boundary layer aerosol. A major result of this earlier work was the identification of sulfur as a component in much of the aerosol collected over mid-ocean regions. At first, the form of the sulfur was unknown, but it was later identified as dimethylsulfide (DMS) which is produced in the upper layer of the ocean by the decay of phytoplankton and is gradually emitted into the atmosphere.

The four year experimental program which is the subject of this report consisted of two sets of measurements made at sea as well as measurements made in the controlled environment of a closed chamber. These three sets of experiments are described below.

DMS Ocean Emission Measurements

The first set of sea measurements had two objectives: (1) to investigate the effects of environmental parameters on the emission rate of DMS from the ocean into the atmosphere, and (2) to track in the atmospheric marine boundary layer the DMS photochemistry that has been observed in laboratory photolysis studies (Hatakeyama et al., 1982 and 1985). These goals were pursued in four field investigations, two in Maine (May and September 1987) where the influence of solar radiation and surface mixing (wave action) on DMS emission rate was measured, one in Bermuda (May 1988) where excellent data on mid-ocean DMS concentrations (in bulk ocean water) and emission rates were collected, and an investigation in coastal waters near San Diego (September 1988) where the influence of the marine microlayer (top mm of the ocean) on DMS emission was studied. These results have been submitted for publication and a copy of the paper is included in Section 4.

Environmental Chamber Measurements

Results of the air chemistry studies in Bermuda showed that it was impossible to interpret the chemical changes occurring with time at a single ocean site in terms of DMS photolysis. The observed changes were strongly influenced by changes in air mass and washout by rain, which occur relatively rapidly so that they completely mask the slower photolytic processes that occur within an individual air mass. As a result, it was decided to investigate the production and growth of aerosol in Calspan's 600 m^3 atmospheric chamber in which DMS was oxidized photochemically to methanesulfonic acid (MSA), SO_2, and ultimately to H_2SO_4. These experiments were performed in clean air and in air with the characteristic reactivity of the atmospheric marine boundary layer.

The growth of MSA aerosol and H_2SO_4 aerosol produced in these chamber experiments was first monitored in high humidity, cloud-free air. To determine the effect of cloud cycling, experiments were performed in which clouds were both produced and dissipated several times. The data collected were to be utilized to study the "Hoppel Hypothesis," which postulates that nonprecipitating cloud cycling enhances aerosol growth rate and leads to a bimodal aerosol size distribution. In additional experiments without cloud formation, photochemical reaction of DMS to MSA, SO_2 and H_2SO_4 was observed and data were collected on product concentrations.

Calspan's role during these experiments was to operate the chamber, manage gas instrumentation and acquire data, both non-computer and computer based. Although NRL also had their own A/D system that acquired and stored data, neither acquisition system was complete, and thus sharing and transfer of data is necessary for each group to acquire a complete data set for analysis. For example, the Calspan system did not record either the aerosol size distributions provided by the NRL mobility analyzer or the condensation nuclei from the NRL condensation particle counter. In addition, the NRL system did not have access to Calspan instrument calibrations nor the zero offsets for each experiment; this information is provided in this report. Also provided are liquid water content measurements made in the fogs produced for the Hoppel Hypothesis experiments, as well as pre- and post-fog concentrations for the gaseous constituents. Chemical ion concentrations are provided for both the DMS photolysis and Hoppel Hypothesis experiments. In addition, this report presents summaries in the form of experiment logs that indicate the experimental setup in terms of input chemical species and controllable conditions, such as ultraviolet illumination and generation of fog. For the photolysis experiments, summary tables that show the purpose of a given experiment, the constituents in the chamber and qualitative results are provided. These tables list the experiments in chronological order. A brief summary of the results for various reactant combinations under dark and illuminated chamber conditions, obtained after an initial "quick-look"

at the data, is provided as well. However, more detailed analysis is required to quantify photolysis rates, branching ratios, etc.

Arabian Sea Haze

In May 1990 another field program obtained aerosol samples to study reduced visibility in haze over the Arabian Sea. A basic description of the aerosol data set acquired and bulk aerosol chemistry of the samples are reported in Section 3. Subsequent Navy sponsoring by the then NOARL Atmospheric Directorate (now NRL Monterey) is funding an ongoing effort to develop a technique to forecast the lowered visibility in this haze, based in part on these previously acquired aerosol samples.

Section 2

EXPERIMENTS IN CALSPAN's 600 m3 CHAMBER

2.1 BACKGROUND AND RATIONALE

The marine boundary layer refers to the air mass directly above the ocean where atmospheric mixing is significant. The upper boundary of this layer is variable but can be considered to extend nominally to about one kilometer above the ocean. This section is concerned with the size distribution and composition of the suspension of fine solid or liquid particles, commonly called aerosols, which are found in this layer, with particular interest focused on sulfur containing aerosols. The oceans are believed to play a significant role in the transport of volatile sulfur compounds from the earth's surface into the atmosphere. Initially, H_2S was thought to be the major compound involved in this transport. However, there is now sufficient evidence to confirm that dimethylsulfide or $(CH_3)_2S$, arising from dimethylsulfoniopropionate in marine phytoplankton, accounts for most of the sulfur transferred from marine environments to the atmosphere.

Over open oceans remote from the influence of land, the aerosol size distribution in the marine boundary layer has been observed to peak in two size ranges between 0.02 and 0.15 μm with a minimum between 0.05 and 0.08 μm (Hoppel et al., 1987). Measurements indicated that the particles under both peaks were too volatile to arise from surface generated sea-salt particles. The peak at the small size was therefore attributed to homogeneous nucleation of new particles from gas-phase reaction products of low volatility. However, the cause of the second peak was still unclear. Hoppel, et. al. (1985), suggested that non-precipitating cloud cycles played an important role in the formation of these double peaks. They made the following argument: Particles in the size range under discussion undergo about ten evaporation/ condensation cycles before removal from the atmosphere by precipitation scavenging. When an aerosol passes through a cloud cycle, the larger particles becomes sites for formation of cloud droplets. Smaller, interstitial particles diffuse to and become part of the droplet while trace gases are absorbed into the droplet where they undergo chemical reactions. When the droplet undergoes a subsequent reevaporation, the aerosol residue is larger than the original particle. Thus, Hoppel argues that the net effect of the nonprecipitating cloud cycle is to produce a minimum in the size distribution of the aerosol particles. The double-peaked feature observed over remote tropical oceans can therefore be attributed to gas-to-particle conversion for both peaks The peak at the small size results from homogeneous nucleation of new particles whereas the peak at about 0.1 μm is the result of gas-phase reactions which occur in cloud droplets during a nonprecipitating cloud cycle (Hoppel, et. al., 1987).

2.1.1 Previous Calspan Chamber Measurements

An initial series of experiments was carried out in Calspan's Environmental Chamber in 1986 in order to test the nonprecipitating cloud cycle hypothesis by measuring the particle size distribution after cycling the aerosol in the chamber through repeated cloud cycles (simulated by repeated compression/expansion cycles in the humidified chamber). As discussed in Hoppel et al. (1987), these experiments were non-definitive in either proving or disproving the hypothesis because of the large loss of cloud droplet due to fallout. The authors pointed out that in the natural environment, these droplets would evaporate back down to aerosol size in the dryer air beneath the cloud. It was suggested at that time that the cloud cycling experiments be repeated with trace gases that are known to promote aqueous phase conversion of absorbed gases so that the conversion occurred on a time scale observable in the chamber. This was essentially the task undertaken in that 1990 set of measurements referred to as the Hoppel Hypothesis Cloud Cycling Experiments.

Also investigated in the environmental chamber at Calspan in 1986 was the role that DMS plays in the initial formation and growth of marine aerosol, i.e., before the aerosol is subjected to cloud cycles. When DMS in the chamber was irradiated with ultraviolet light (simulated sunlight), a large number of very small particles was formed which continued to grow as long as the irradiation continued. Analysis of the particle size distributions and their respective growth rates suggested the following interpretation. The photooxidations of DMS (CH_3SCH_3) result in products of extremely low volatility, most likely methane sulfonic acid (CH_3SO_3H) and sulfuric acid (H_2SO_4), whose initial concentration is so large that homogeneous nucleation of new particles occurs.* After enough particle surface is generated, condensation of the material on existing particles begins, thereby lowering its concentration below the homogeneous nucleation limit. Growth of existing particles continues as long as the photooxidation produces condensable material. The objective of the photolysis experiments in the 1990 chamber measurements described in this report was to further examine the chemistry of the gas-to-particle conversion which occurs upon irradiation of DMS in the presence of oxidizers.

* Homogeneous nucleation is the spontaneous formation of new particles directly from supersaturated vapor. The higher the supersaturation, the smaller will be the radius of the critical size nucleus. If the nucleation process involves more than a single molecular species, then the nucleation is hetermolecular. Heterogeneous nucleation refers to the nucleation of previously existing particles. The nucleation is referred to as binary heterogeneous nucleation if the supersaturation is with respect to a binary solution

2.1.2 1990 Chamber Measurements - Objectives and Rationale

2.1.2.1 Photooxidation Mechanisms

The remote marine atmosphere contains a variety of trace gases which are important to the understanding of the DMS mechanism. These gases include O_3 (typical concentrations about 20 ppb) whose source is believed to be mostly downward mixing from the upper atmosphere with only a small contribution arising from local photolysis. Ultraviolet irradiation of the O_3 and subsequent reaction of $O(^1D)$ with water, results in formation of the hydroxyl radical, OH, one of the prime oxidizers of DMS.* Typical rates of OH formation in the atmosphere are of the order of 1×10^6 molecules/cc/sec averaged over 24 hours or about 5×10^6 molecules/cc/sec at noontime (Hoppel private communication). This production rate is significant. However, due to the high reactivity of OH, its lifetime is only about 1 second**. The concentration of OH in the atmosphere is therefore about 1×10^6 molecules/cc

One issue regarding the initial oxidation of DMS with OH is the extent of competition between addition and abstraction pathways. The addition pathway produces the adduct $CH_3S(OH)CH_3$ while the abstraction (of hydrogen) pathway leads to CH_3SCH_2. Yin et al. (1990) concluded in their study that for the reaction of OH with organosulfur compounds, addition is the dominant pathway. However, because of the reverse decomposition reaction of the addition adduct. the *effective or apparent* pathway can be dominated by abstraction at temperatures greater than 285K.

A more critical issue in understanding the mechanism of DMS oxidation is the subsequent reaction of the primary adducts and the impact of secondary reactions with other trace species. It has been observed for example, that the presence of NO_2 increases the rate of reaction of OH with DMS (Yin et al., 1990). The degree to which the presence of NO_2 impacts the relative amounts of MSA and sulfuric acid products is an open question. Figure 1 outlines a proposed mechanism for the atmospheric photooxidation of DMS (Ibid). As indicated in the figure, both the addition and abstraction pathways can lead to methane sulfonic acid (CH_3SO_3H) (MSA) and SO_2, the latter then undergoing conversion to H_2SO_4. Note that NO_2 reactions play a role in many of the proposed reaction paths

Other trace gases which are present in the remote marine boundary layer include hydrocarbons such as propane, propene, ethane and ethene. These hydrocarbons are injected into the atmosphere at a rate of about 0.5 $\mu g/hr\text{-}m^2$ from the ocean (Private communication, W. Hoppel, Sept. 10, 1990). Propene is

---

* Other oxidizers believed to play a role in DMS oxidation include $O(^3P)$, NO_3 and IO radicals

** The primary loss mechanisms are through oxidation of CO and methane with CO being the larger sink. Filtering of the chamber air is critical for removal of the CO. The activated charcoal will not remove methane, however. Ambient concentrations of methane (rural) are about 2 5 ppm

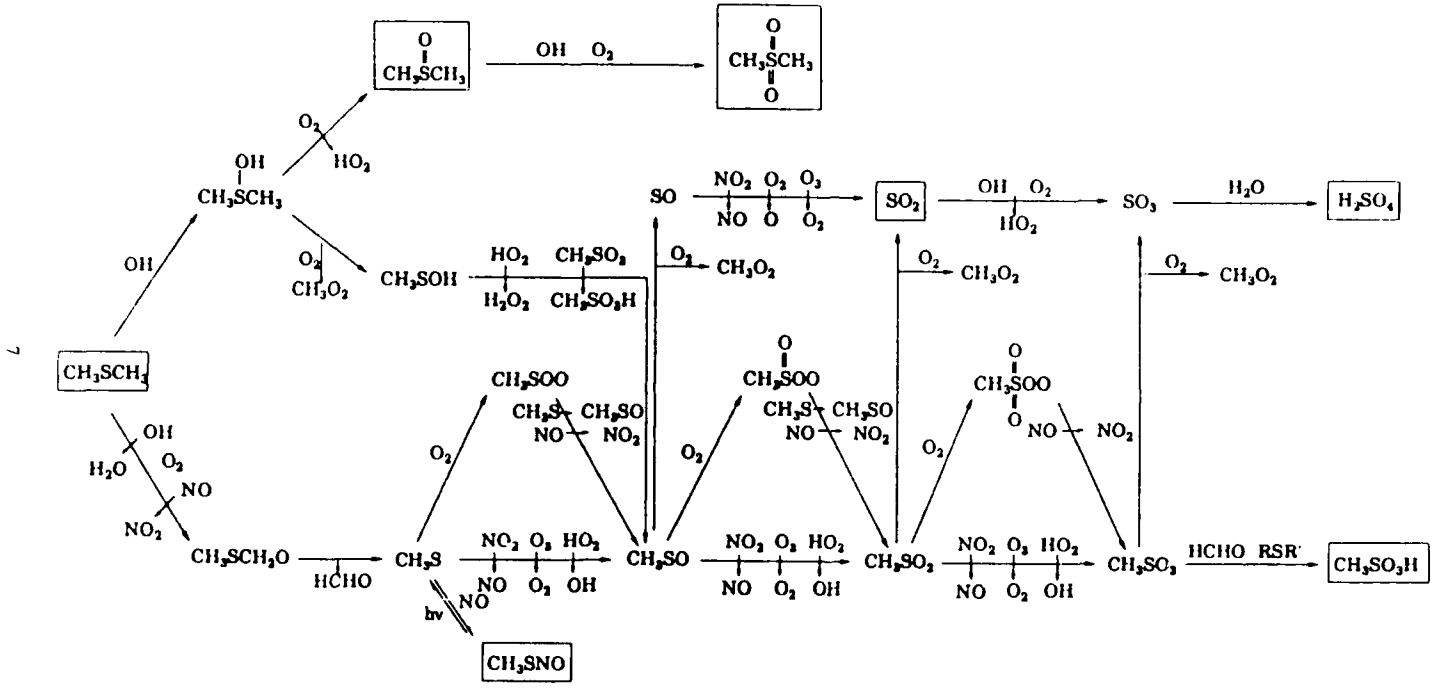

Figure 1 CH_3SCH_3 ATMOSPHERIC PHOTOOXIDATION MECHANISM (Yin et al., 1990)

believed to be the most reactive with respect to OH and O_3 and is one of the trace gases used in the current study.

During the cloud phase, a droplet can absorb oxidizers along with soluble trace gases such as SO_2 (from the oxidation of DMS) and NH_3, which then react within the liquid droplet at a rate which depends on the pH of the droplet. For example, as the pH of the droplet decreases (becomes more acidic), the in-cloud conversion of SO_2 to sulfate slows. The products of these in-cloud oxidation reactions with SO_2 and NH_3 (MSA, H_2SO_4, $(NH_4)_2SO_4$) are less volatile than the reactants and therefore leave a larger particle residue after the cloud droplet evaporates. The size distribution of the particles as well as the effects of droplet pH on the growth of the droplets are the subject of the chamber experiments described in this report.

2.1.2.2 Hoppel Hypothesis - Cloud Cycling Experiments

As stated earlier, the bimodal size distribution observed at sea was not observed in the 1986 chamber experiments. In those experiments, DMS, which itself is insoluble in the cloud droplets, was used as the starting point. It is believed that the bimodal distribution was not observed because the photolysis of DMS was slow relative to the test time available in the chamber and the subsequent fallout of cloud droplets made quantitative measurements difficult. During the experiments discussed in this report, the starting point for the attempt to generate the bimodal size distribution was not DMS, but one of the major gaseous products of DMS oxidation, namely SO_2. The objectives of the cloud cycling experiments can be summarized as follows:

1. Measure the change in aerosol size distribution caused by the conversion of gaseous SO_2 to sulfate in cloud droplets during a cloud cycle. Generate, if possible, the double peaked aerosol size distribution observed in nature. Introduce low levels (ppb) of SO_2 and a representative oxidizer (O_3, H_2O_2). Check residual aerosol and if necessary, briefly turn on lights to generate an initial aerosol distribution. Measure aerosol size distribution after several repeated cloud cycles.
2. Examine (at least qualitatively) the SO_2 conversion to sulfate by oxidation with O_3 and H_2O_2. By adding gaseous NH_3 and repeating cloud cycling experiments, examine the hypothesis that pH has dramatic effects on oxidation by O_3.
3. Create a realistic, reactive atmosphere and perform illumination and cloud cycling experiments.

2.1.2.3 Photolysis Experiments

The approach taken in the photolysis experiments was to sequentially add to a clean chamber the gaseous components believed to be important in the remote marine atmosphere, keeping the concentrations on the high side of the range expected in the marine environment. The overall objective was to investigate the gas phase photolysis rate of DMS and the gas to particle conversion which occurs upon irradiation of DMS in the marine atmospheric environment:

1. Add to DMS–containing atmosphere various oxidizers alone and in combination, such as O_3, NO, O_3 + NO, and H_2O_2. Examine effect on SO_2 production and sulfate, MSA and nitrate yields.
2. Add propene (CH_2=$CHCH_3$) to the system and study the increase in SO_2 oxidation in the ozone/alkene mixture. The oxidation of SO_2 is thought to involve Criegee intermediates.
3. Add ammonia (NH_3) to the SO_2 photolysis experiments and monitor particle formation to determine if gas phase sulfamic acid (NH_3SO_3) is condensing into embryos which evolve into nucleation sites. Examine impact of pH.

2.2 CALSPAN'S ENVIRONMENTAL TEST CHAMBER, ASHFORD, NY

Calspan's Ashford test chamber was originally designed as part of an ordnance test facility. Extensive modifications have been made over the past few years, converting it to a unique facility for atmospheric simulation, air pollution, cloud physics and aerosol research studies. Relevant facility characteristics are described below:

(1) Physical Characteristics

The heart of the test facility is a cylindrical chamber of 9m diameter and 9m height. The total volume is 600m^3 (20,000 ft^3), making it one of the largest available test chambers in the United States, especially valuable in minimizing wall effects and closely simulating actual atmospheric conditions. The chamber wall is constructed of 0.5-inch plate steel designed for pressure differentials up to 9 psig. Figure 2 presents a cutaway view of the entire facility. Figure 3 (chamber schematic) and Figure 4 (floor plan) show the chamber location relative to the auxiliary facilities housed in the same laboratory complex. An interior view of the chamber is shown in Figure 5.

(2) Chamber Surface

The inner chamber surface is covered with a special coating developed at the United States Naval Research Laboratory. This coating material is a highly fluorinated epoxy-polyurethane copolymer. The *in situ* curing of the polyurethane base enables good adhesion to the chamber surface. The very high fluorine content provides, in analogy to fluorocarbon polymers, both high chemical stability and low surface energy. Such favorable physical and chemical characteristics add further to the capability of the chamber in minimizing possible wall effects during photochemical aerosol studies.

(3) Air Purification

A schematic diagram of the chamber air ventilation system is shown in Figure 3. Absolute filters are incorporated to permit virtually total removal of particulates (< 200 Aitken nuclei/cm^3). Impregnated charcoal filter panels (not shown in Figure 3) are installed to enable the removal of gaseous contaminants. Some of the most difficult to remove contaminants, such as CO and CH_4, are present only at minimum concentrations in the unpurified ambient air due to the rural location of the test facility (about 35 miles south of Buffalo, New York). The air purification system is thus capable of preconditioning the chamber for studies of pollutant effects even at minute concentrations.

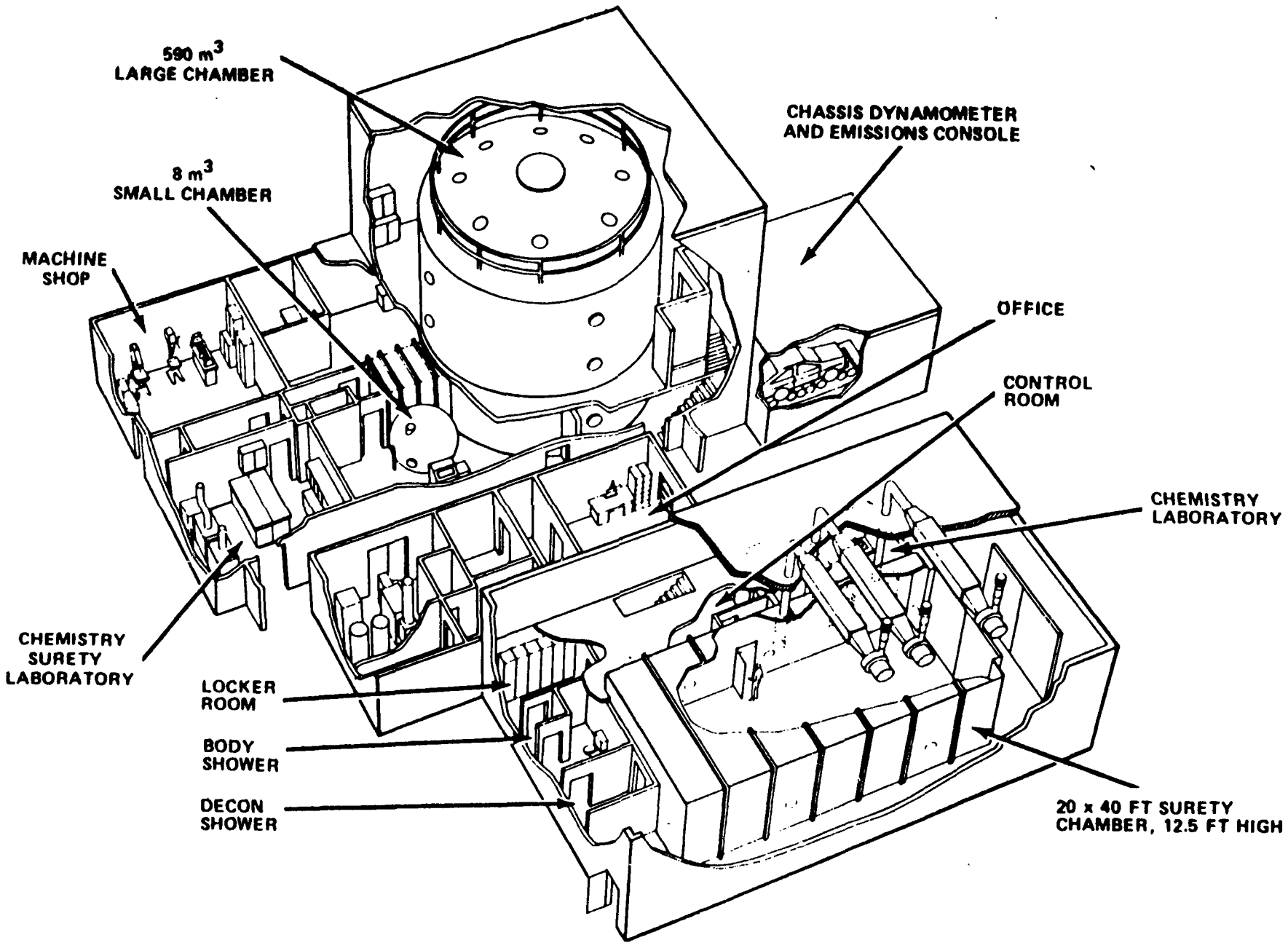

Figure 2 CUT-AWAY VIEW OF CALSPAN'S ASHFORD FACILITY

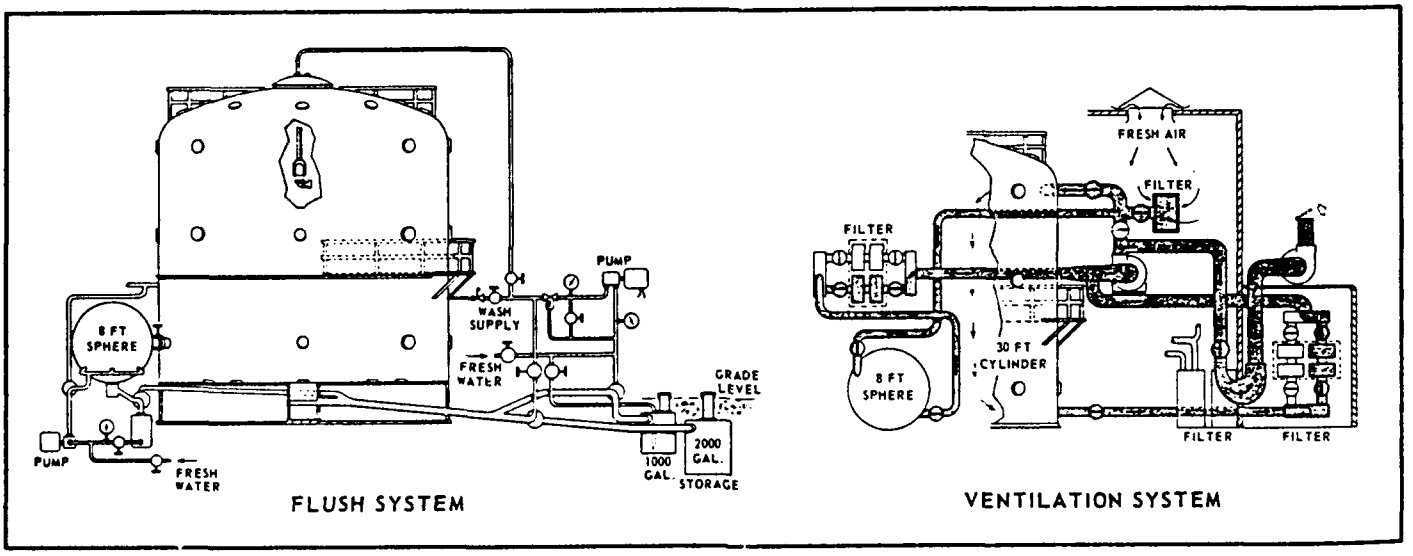

Figure 3 CHAMBER SCHEMATIC

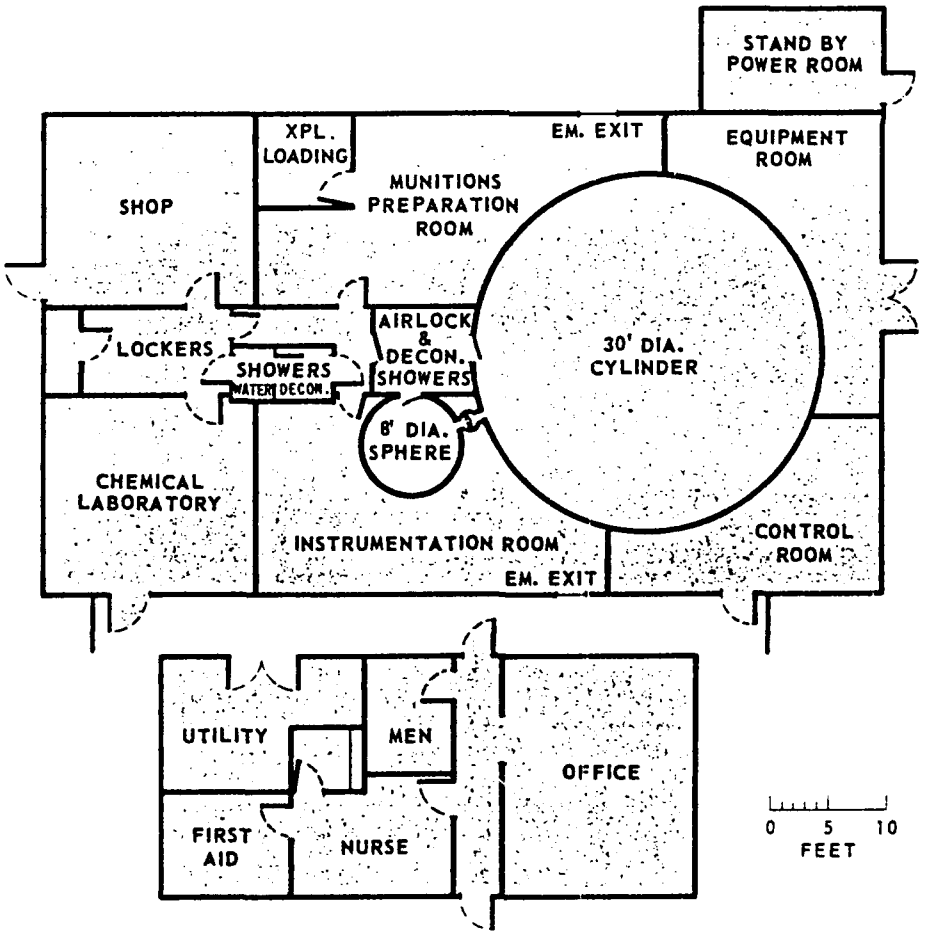

Figure 4 FLOOR PLAN OF CHAMBER FACILITY

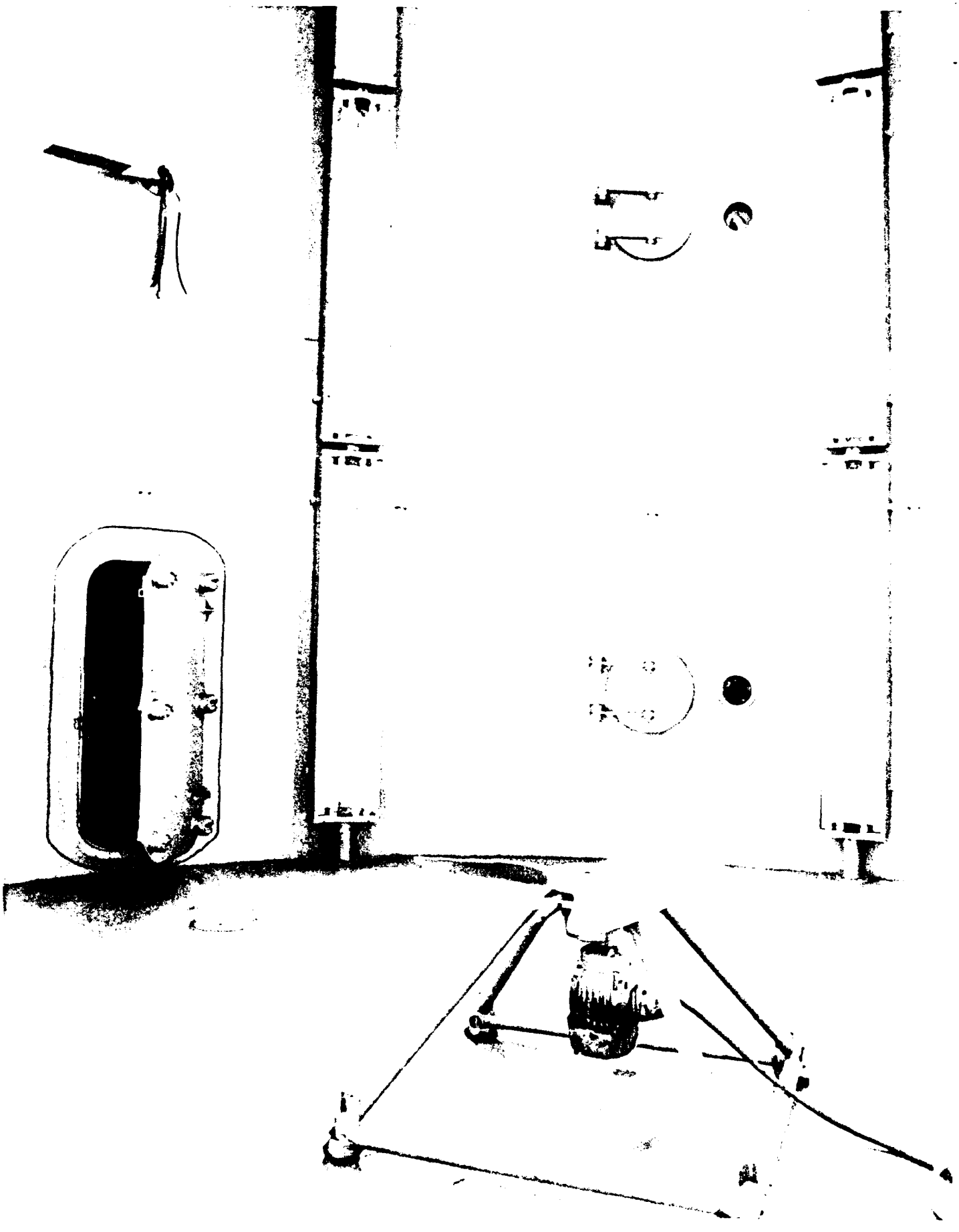

Figure 5 INTERIOR VIEW OF THE CHAMBER

(4) Air Humidity Control

Humidistatically controlled cooling coils installed in the ductwork in series with the absolute filters serve to dehumidify the chamber air. Humidity increases are achieved by spraying distilled water from nozzles installed around the perimeter of the chamber ceiling.

(5) Liquid Flushing System

The chamber is equipped with a water flush system as shown schematically in Figure 3. Prepurified water with or without addition of a detergent can be introduced into the chamber through a rotating jet sprayer. This flush system reaches all areas of the chamber wall, provides for a very effective surface cleaning, and may also be utilized on some occasions for gross adjustment of humidity.

(6) Photo-irradiation Sources

Photolysis lamps simulating the near UV portion of the earth's ground level solar radiation spectrum are located around the chamber wall to permit near uniform intensity distribution within the chamber. Twenty-four individual light fixtures, each containing two special Sylvania high-intensity blacklight lamps, two 215W fluorescent GE sunlamps, and eight GE-F72T12/HO/BL blacklight lamps are arranged in three horizontal rows and eight vertical columns radially spaced equally along the chamber wall. Each of the light source combinations is encased in a gas-tight enclosure equipped with a 15" x 96" Pyrex glass front panel. Forced air cooling (separated from the chamber air) is used to minimize possible temperature rises at these light source fixtures. Some of the light fixtures may be seen in Figure 5, which shows an inside view of the chamber. Gentle stirring at low rpm by the fan in the foreground prevents the formation of inhomogeneities that would be caused by unavoidable light intensity and temperature gradients in stagnant air.

(7) Instrumentation

The principal instrumentation provided and operated by Calspan were:

- Meloy sulfur analyzer for monitoring total gaseous sulfur (primarily DMS) in chamber. See calibration curve in Figure 6.
- Bendix nitrogen oxides analyzer for measuring concentrations of NO and NO_x.
- Bendix ozone analyzer for monitoring ozone concentration.

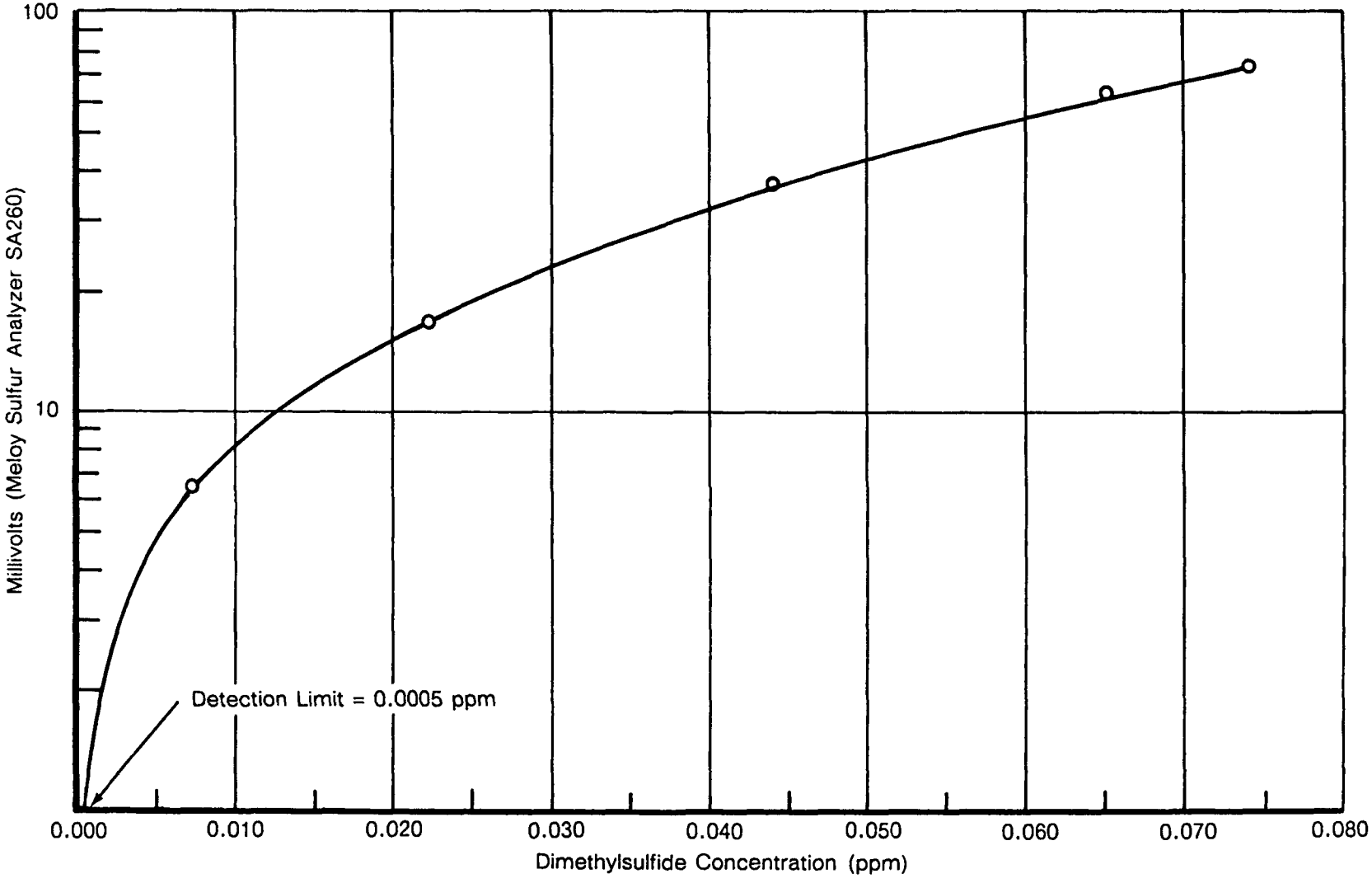

Figure 6 CALIBRATION OF MELOY TOTAL SULFUR ANALYZER SA260 OCTOBER 25, 1990

- Reactive hydrocarbon analyzer for monitoring gross levels in the chamber. [Reactive hydrocarbons determine the overall reactivity in the chamber and must be controlled to be characteristic of the marine boundary layer.]
- Filtration equipment for collection of aerosol samples for chemical analysis for MSA, $SO_4^=$ and NO_3^-.
- DEW-ALL for monitoring relative humidity.
- IR transmissometer for continuously monitoring liquid water content.

NRL provided and operated the mobility analyzer for determining aerosol size distribution, a TSI model 3022 condensation particle counter for measuring condensation nuclei (CCN) and Thermal Environmental Instruments Inc. Model 43S High Sensitivity Pulsed Flourescence SO_2 Analyzer.

The SO_2, ozone and non-methane hydrocarbon instruments were very stable and these data can be used with confidence for both sets of experiments. Conversely, the total sulfur analyzer had problems working at the saturated and nearly saturated humidities utilized in the Hoppel Hypothesis experiments However, the only gaseous sulfur species present was SO_2, which was monitored by the NRL SO_2 analyzer.

On the other hand, the total sulfur analyzer was needed to measure the DMS concentration in the DMS photolysis experiments. Fortunately, these experiments were run at moderate to low relative humidities at which the instrument functioned well. The reported DMS values were obtained by subtracting the SO_2 concentration from the measured total sulfur values.

Since the concentrations of NO/NO_X which were used were near the lower limit of the instrument, it was usually zeroed just before injection of NO into the chamber. Because of instrument drift, interpretation of measured time sequences of NO/NO_X in terms of experimental time histories is questionable. However, zeroing the instrument just before injection of the species into the chamber provided confidence in the measured input concentration.

2.3 HOPPEL HYPOTHESIS EXPERIMENTS

This section provides a description of the experimental approach as well as summary material for the cloud chamber experiments in the form of experiment logs, zero offsets for instruments, and experimental values for ion species concentrations and fog liquid water content.

2.3.1 Experimental Approach and Data Acquired

A typical Hoppel Hypothesis experiment day began with the termination of the overnight filtering of the chamber air. This filtering removed both gases and particulates from the air. Instrumentation was checked out in preparation for the day's experiments, including zero adjustments and full-scale (span) settings. Next, selected chemicals were added and uv-irradiated if required to create an initial aerosol distribution. Utilizing the aerosol as condensation nuclei, a fog was then formed and liquid water content measurements were made. The fog was subsequently evaporated and the size distribution of the resultant dry aerosol was measured. Depending on experiment protocol, this procedure was carried out for up to as many as five fogs per day. The details of these steps are outlined below:

1) form proper initial dry aerosol size distribution by adding combinations of SO_2, O_3 and/or H_2O_2 into uv-irradiated or dark chamber. The "correct" size distribution was assessed from NRL mobility analyzer data.

2) increase the SO_2 concentration in the chamber air just prior to fog formation to provide excess SO_2 for conversion to sulfate in fog droplets.

3) form fog by expansion of pressurized chamber containing very high relative humidity air.

4) measure liquid water content (LWC) of fog using IR transmissometer.

5) recompress chamber air to dissipate fog to get post-fog drysize distribution. This procedure was utilized, because if fog was allowed to dissipate naturally by the long-term process of transfer of heat from chamber walls, droplets would fall out and cloud condensation nuclei would then be lost to subsequent cycles.

6) collect a filter sample for Calspan chemical particulate analyses ($SO_4^=$, NO_3^- and MSA).

7) add desired chemicals to chamber (Step 2).

8) make new fog (Step 3).

At the end of the day's experiments, the chamber was flushed with ambient, outside air. Just before departure for the day, the fresh air flush was terminated, the chamber was sealed and its air circulation

system was set to filter this ambient air sample overnight to produce the clean atmosphere for the next day's experiments.

2.3.1.1 Experiment Logs

In the experiment logs (Table 1), the thirteen experiment days are numbered consecutively by calendar day. On a given day, data are provided for each fog that was generated on that day. For each setup, the checkmarks show the chemical constituents added to produce the aerosol distribution on which and the chamber atmosphere in which the individual fog (cloud) was produced, as well as indicating whether UV irradiation took place. For the first fog of the day (Fog 1), the checkmark indicates material added prior to fog formation. For subsequent fogs, a checkmark indicates that the species was added to the chamber atmosphere that remained after recompression to evaporate the preceding fog. Presence of ion chromatograph and liquid water content data are indicated, and comments are included where warranted.

2.3.1.2 Zero Offsets

Zero offsets or baseline values are shown in Table 2 for the instruments required for the Hoppel Hypothesis experiments summarized in Table 1. Nitrogen gases were not used in these experiments. Data for the total sulfur analyzer are not shown for two reasons: 1) the only gaseous sulfur species present was SO_2, which was monitored by the NRL SO_2 analyzer and 2) the instrument had problems working at the saturated and nearly saturated humidities utilized in these experiments.

The SO_2 and ozone instruments were very stable as shown by the daily offset values and consequently these zero offsets have been removed from the recorded data to obtain the values reported in Table 3. On the other hand, while the non-methane hydrocarbon analyzer was also stable, different offset values occurred because of varying background levels in the chamber. Hence, values reported in the table are those background levels, and examination of any NMHC species input for a given experiment requires removal of the background value.

2.3.1.3 Pre- and Post-Fog Values

Fogs were formed in the chamber by first pumping air into the chamber thereby compressing the resident chamber air [Compression (1)] while maintaining relative humidity just under 100%. The chamber air was then allowed to expand (by opening a port) producing supersaturation and fog. A subsequent compression [Compression (2)] evaporated the fog and left the aerosol population as condensation nuclei for the next fog. The basic data acquisition schedule provided values just prior to beginning Compression (1) and just after ending Compression (2). However, upon examining the data output, it was apparent

Table 1
LOG OF HOPPEL HYPOTHESIS EXPERIMENTS

			INPUTS							
Experiment Day	Date	Test	SO_2	O_3	H_2O_2	UV	Other	Ion Data	Liquid Water	Comments
1	10/29	Set-up	√			√		√		Pre-fog Size Distribution Test
2	10/30	Set-up	√			√		√		
		Fog 1	√		√			√	√	
		Fog 2	√		√			√	√	
		Fog 3	√		√			√	√	
3	10/31	Set-up	√		√	√				
		Fog 1	√		√			√	√	
		Fog 2	√					√	√	
		Fog 3	√	√				√	√	
4	11/1	Set-up	√	√						
		Fog 1	√	√				√	√	
		Fog 2	√					√	√	
		Fog 3		√			NH_4OH	√	√	
5	11/2	Set-up	√	√						
		Fog 1	√	√				√	√	
		Fog 2	√	√				√	√	
		Fog 3		√				√	√	
		Fog 4	√	√			NH_3	√	√	
		Fog 5		√			NH_3	√	√	

Table 1
LOG OF HOPPEL HYPOTHESIS EXPERIMENTS (cont.)

			INPUTS							
Experiment Day	Date	Test	SO_2	O_3	H_2O_2	UV	Other	Ion Data	Liquid Water	Comments
6	11/3	Set-up	√	√				√		
		Fog 1	√	√				√	√	
		Fog 2						√	√	
		Fog 3		√			NH_3	√	√	
7	11/9	Set-up	√	√		√	Propylene			
		Fog 1	√	√			Propylene	√	√	
		Fog 2	√	√				√	√	
		Fog 3	√	√			NH_3	√	√	
		Fog 4						√	√	Chamber Fresh Air Flushed. Ambient Nuclei
		Fog 5	√	√				√	√	Ambient Nuclei
8	11/10	Set-up	√	√	√		Propylene			
		Fog 1	√	√	√		Propylene	√	√	
		Fog 2							√	
		Fog 3	√		√			√	√	
9	12/3	Set-up	√	√		√				
		Fog 1	√	√				√	√	
		Fog 2	√	√				√	√	

Table 1
LOG OF HOPPEL HYPOTHESIS EXPERIMENTS (cont.)

			INPUTS							
Experiment Day	Date	Test	SO_2	O_3	H_2O_2	UV	Other	Ion Data	Liquid Water	Comments
10	12/4	Set-up	√	√		√				
		Fog 1	√	√				√	√	
11	12/5							√		Conditions after Overnight Decay
		Set-up	√	√		√				
		Fog 1	√	√				√	√	
		Fog 2			√			√	√	
		Fog 3	√	√				√	√	
12	12/6	Set-up	√		√	√				
		Fog 1	√		√			√	√	
13	12/7	Set-up		√		√	DMS			8 hour photolysis
		Fog 1	√	√			DMS	√		

Table 2
HOPPEL HYPOTHESIS EXPERIMENTS, INSTRUMENT ZERO OFFSETS

Date (1990)	Time	SO_2 (ppb)	O_3 (ppm)	NMHC (ppm)
10/29	1850	1.5	0.001	0.260
10/30	1650	*	±0.000	1.36
10/31	1452	*	+0.0013	3.19
11/1	0848	1.56	—	1.91
11/1	1048	—	+0.001	—
11/2	0845	1.3	+0.001	1.34
11/3	0935	*	+0.001	1.24
11/9	0905	-1.0	+0.001	0.74
11/9	1242	1.1		
11/10	0918	0.7	+0.0008	1.03
12/3	0916	—	+0.0004	—
12/3	1100	—		1.76
12/3	1147	1.7		
12/4	0908	—	+0.0005	0.64
12/4	1100	1.5		
12/5	1344	1.3	+0.0005	3.21
12/5	1504			4.00
12/6	1226	1.3	+0.0005	4.00
12/7	1633 (12/6)	1.5	+0.0007	3.80

* No overnight filtering and instrument levels reflect concentrations from previous day's experiments. Therefore, use zero offsets from previous day

that the SO_2 concentration showed noticeable variations at other points along the experimental time line. Thus, Table 3 presents values not only for the beginning and end points of a particular fog, but also for any intervening points at which potentially significant changes appeared to occur.

2.3.1.4 Chemical Composition of Aerosol

Table 4 shows the chemical composition of the aerosol which existed at the completion of a cloud cycle. The aerosol was collected on a filter which was exposed for approximately 8–10 minutes at a nominal flow rate of 30 cubic feet per minute. The collected aerosol was then leached from the filter with deionized water. The resulting solution was filtered and then injected into an ion chromatograph from which the concentrations of the various ions reported in Table 4 were obtained.

2.3.1.5 Fog Liquid Water Content

Table 5 shows the liquid water content of the fogs (cloud) generated in the chamber. These values were obtained by Chylek's method (1978) by measuring IR extinction at 11 μm over a 18 m path length (a double traverse of the chamber diameter obtained by reflecting the IR beam at the opposite wall).

2.3.2 Discussion

The data for these Hoppel Hypothesis Experiments have been analyzed and the results initially appeared in a paper presented at the American Association for Aerosol Research 1991 annual conference (Hoppel et al., 1991). Details of these analyses can be found in a companion report (Frick et al , 1992). These analyses show that under the chamber conditions in which the pre-cloud SO_2 and ozone concentrations could be carefully controlled, the size distributions taken before and after a cloud cycle show significant conversion of SO_2 to H_2SO_4 and a dramatic change in the aerosol size distribution. These results constitute strong evidence for the validity of the Hoppel Hypothesis.

Table 3
HOPPEL HYPOTHESIS EXPERIMENTS PRE- AND POST- FOG VALUES

Date Event	Time	SO_2 (ppb)	NMHC (ppm)	O_3 (ppb)
10/30/90	1651 Begin Compression (1)	4.0	1.36	0.0
Fog (1)	1701 End Compression (1)	6.4	1.38	0.0
	1719 End Compression (2)	5.7	1.36	0.0
	1745 Begin Compression (1)	6.1	1.39	0.0
	1750 Peak SO_2	8.3	1.38	-
Fog (2)	1756 End Compression (1)	7.4	1.40	-
	1814 End Compression (2)	5.9	1.45	0.0
	1840 Begin Compression (1)	7.5	1.51	0.0
	1843 Peak SO_2	8.1	1.50	-
Fog (3)	1851 End Compression (1)	6.9	1.50	-
	1912 End Compression (2)	6.0	1.56	0.0
10/31/90	1500 Begin Compression (1)	9.4	3.22	0.0
Fog (1)	1510 End Compression (1)	6.2	3.21	0.0
	1520 Experiment End	5.0	3.26	0.0

Table 3
HOPPEL HYPOTHESIS EXPERIMENTS PRE- AND POST- FOG VALUES (cont.)

Date Event	Time	SO_2 (ppb)	NMHC (ppm)	O_3 (ppb)
10/31/90	1559 Begin Compression (1)	10.6	3.33	0.0
Fog (2)	1610 End Compression (1)	7.2	3.36	0.0
	1617 End Compression (2)	6.5	3.37	0.0
	1705 Add SO_2	11.5	3.49	0.0
Fog (3)	1715 Add O_3	8.2	3.50	297
	1813 Begin Compression (1)	7.9	3.60	206
	1840 End Compression (2)	8.6	3.46	165
11/1/90	1536 Begin Compression (1)	7.2	2.29	123
	1538 Maximum SO_2	7.6	2.28	121
Fog (1)	1548 End Compression (1)	6.2	2.25	110
	1605 End Compression (2)	4.7	2.21	97
Fog (2)	1645 Begin Compression (1)	5.2	2.29	77
	1712 End Compression (2)	5.1	2.19	62
Fog (3)	1835 Begin Compression (1)	7.1	2.41	86
	1902 End Compression (2)	7.5	2.37	72

Table 3
HOPPEL HYPOTHESIS EXPERIMENTS PRE- AND POST- FOG VALUES (cont.)

Date Event	Time	SO_2 (ppb)	NMHC (ppm)	O_3 (ppb)
11/2/90	1312 Begin Compression (1)	6.2	1.80	89
Fog (1)	1345 End Compression (2)	4.2	1.82	70
	1453 Begin Compression (1)	8.9	2.02	84
Fog (2)	1503 End Compression (1)	6.9	2.02	78
	1520 End Compression (2)	6.3	2.09	70
	1553 Begin Compression (1)	10.0	2.20	94
Fog (3)	1602 End Compression (1)	8.1	2.19	87
	1626 End Compression (2)	7.6	2.19	78
Fog (4)	1716 Begin Compression (1)	7.5	2.35	84
	1743 End Compression (2)	7.5	2.35	72
Fog (5)	1810 Begin Compression (1)	7.7	2.44	101
	1820 End Compression (2)	8.0	2.42	85

Table 3
HOPPEL HYPOTHESIS EXPERIMENTS PRE- AND POST- FOG VALUES (cont.)

Date Event	Time	SO_2 (ppb)	NMHC (ppm)	O_3 (ppb)
11/3/90	1219 Begin Compression (1)	5.9	1.40	88
Fog (1)	1246 End Compression (2)	5.9	1.43	78
Fog (2)	1316 Begin Compression (1)	6.0	1.49	70
	1343 End Compression (2)	6.3	1.49	61
Fog (3)	1439 Begin Compression (1)	6.5	1.70	91
	1504 End Compression (2)	6.6	1.62	81
11/9/90	1309 Begin Compression (1)	6.4	1.87	93
Fog (1)	1337 End Compression (2)	2.1	1.78	69
Fog (2)	1439 Begin Compression (1)	5.0	1.82	98
	1505 End Compression (2)	1.6	1.77	98
Fog (3)	1556 Begin Compression (1)	1.3	1.84	93
	1626 End Compression (2)	1.0	1.80	63

Table 3
HOPPEL HYPOTHESIS EXPERIMENTS PRE- AND POST- FOG VALUES (cont.)

Date Event	Time	SO_2 (ppb)	NMHC (ppm)	O_3 (ppb)
11/9/90	1915 Begin Compression (1)	0.8	1.72	1.4
Fog (4)	1942 End Compression (2)	0.7	1.75	0.8
Fog (5)	2012 Begin Compression (1)	6.5	1.82	83
	2022 End Compression (1)	4.9	1.80	76
	2040 End Compression (2)	2.9	1.82	64
11/10/90	1220 Begin Compression (1)	4.3	1.33	17.3
	1231 End Compression (1)	2.9	1.36	15.0
Fog (1)	1235 In fog	4.2	1.36	-
	1246 End Compression (2)	2.2	1.38	13.1
Fog (2)	1352 Begin Compression (1)	0.9	1.50	7.3
	1413 End Compression (2)	0.8	1.54	6.1
Fog (3)	1430 Begin Compression (1)	0.9	1.59	4.8
	1440 End Compression (1)	6.1	1.59	4.3
	1446 Begin Compression (2)	4.3	1.63	4.0

Table 3
HOPPEL HYPOTHESIS EXPERIMENTS PRE- AND POST- FOG VALUES (cont.)

Date Event	Time	SO_2 (ppb)	NMHC (ppm)	O_3 (ppb)
12/3/90	1509 Begin Compression (1)	0.2	6.49	1.73
Fog (1)	1532 End Compression (1)	0.3	7.30	122
	1552 End Compression (2)	0.2	7.24	98
Fog (2)	1707 Begin Compression (1)	0.4	7.45	212
	1738 End Compression (2)	0.5	7.14	153
12/4/90	1547 Begin Compression (1)	2.1	1.82	193
	1603 End Compression (1)	1.0	1.82	175
Fog (1)	1613 Begin Compression (2)	0.8	1.89	166
12/5/90	1344 Begin Compression (1)	2.1	3.20	98
Fog (1)	1406 Begin Compression (2)	2.0	3.14	87
	1506 Begin Compression (1)	2.1	4.03	67
Fog (2)	1527 Begin Compression (2)	2.1	4.05	62
Fog (3)	1703 Begin Compression (1)	2.1	3.09	64
	1719 End Compression (1)	0.9	3.07	239
	1732 Begin Compression (2)	0.7	3.15	229

Table 3
HOPPEL HYPOTHESIS EXPERIMENTS PRE- AND POST- FOG VALUES (cont.)

Date Event	Time	SO_2 (ppb)	NMHC (ppm)	O_3 (ppb)
12/6/90	1226 Begin Compression (1)	3.8	4.00	1.70
Fog (1)	1341 End Compression (1)	5.8	3.95	1.50
	1247 UV ON	5.9	3.95	1.75
12/7/90	1316 Begin Compression (1)	1.1	N/A	257
Fog (1)	1327 End Compression (1)	5.0	N/A	233
	1334 Begin Compression (2)	5.0	N/A	223

Table 4
CHEMICAL CONSTITUENTS FOR HOPPEL HYPOTHESIS EXPERIMENTS

Sample No.	Date	Time	Volume Sampled (m^3)	MSA ($\mu g/m^3$)	SO_4^{--} ($\mu g/m^3$)	NO_3^- ($\mu g/m^3$)	NH_3 ($\mu g/m^3$)
1	10/30	1011-1016	4	-	<0.3	-	-
2	10/30	1710-1720	5.6	-	2.5	-	-
3	10/30	1805-1915	5.6	-	4.0	-	-
4	10/30	1903-1913	5.6	-	8.3	-	-
5	10/31	1525-1534	5.6	-	3.0	-	-
6	10/31	1617-1627	6.4	-	2.2	-	-
7	10/31	1757-1806	5.6	-	1.4	-	-
8	11/1	16222-1631	5.6	-	2.6	-	-
9	11/1	1720-1729	5.6	-	2.8	-	-
10	11/1	1910-1919	5.7	-	1.2	-	<0.02
11	11/2	1347-1356	5.8	-	2.5	-	-
12	11/2	1422-1431	5.7	-	1.2	-	-
13	11/2	1529-1538	5.7	-	1.2	-	-
14	11/2	1632-1641	5.7	-	4.0	-	-
15	11/2	1750-1759	5.7	-	3.1	-	<0.02
16	11/2	1842-1851	5.7	-	4.	-	<0.02
17	11/3	1110-1119	5.7	-	3.3	-	-
18	11/3	1131-1137	5.7	-	1.4	-	-
19	11/3	1250-1257	5.7	-	2.1	-	-
20	11/3	1348-1354	5.7	-	2.0	-	-
21	11/3	1506-1515	5.7	-	2.6	-	-
26	11/9	1346-1352	5.7	-	2.5	0.35	-
27	11/9	1516-1524	7.5	-	4.34	0.56	-

Table 4
CHEMICAL CONSTITUENTS FOR HOPPEL HYPOTHESIS EXPERIMENTS (cont.)

Sample No.	Date	Time	Volume Sampled (m^3)	MSA ($\mu g/m^3$)	SO_4^{--} ($\mu g/m^3$)	NO_3^- ($\mu g/m^3$)	NH_3 ($\mu g/m^3$)
28	11/9	1633-1644	8.4	-	9.96	0.69	+0.05
				Background Natural Nuclei			
29	11/9	1816-1830	12.7	-	2.89	0.43	-
30	11/9	1947-1958	9.2	-	0.93	<0.02	-
31	11/9	2044-2054	8.8	-	4.0	1.4	-
32	11/10	1255-1305	8.96	-	11.3	0.47	-
33	11/10	1504-1513	6.6	-	7.13	0.44	-
48	12/3	1607-1619	11.7	<0.05	2.47	0.56	
49	12/3	1802-1812	9.4	<0.05	3.53	0.80	
50	12/4	1640-1650	9.4	0.13	1.32	0.34	
51	12/5	0845-0858	10.2	<0.01	0.86	0.28	
52	12/5	1430	Blank Filter	0.2	1.7	2.1	Total in Filter
53	12/5	1440	8.5	<0.01	0.59	0.25	
54	12/5	1545	8.5	<0.01	0.78	<0.1	
55	12/5	1800	8.5	<0.01	0.78	<0.1	
CW	12/5	1840	Chamber Water	<0.2	1.96	0.14	
56	12/6	1330	11.0	0.04	1.26	0.16	($\mu g/ml$)
CW	12/6	1500	Chamber Water	<0.2	1.15	0.18	($\mu g/ml$)

Table 5
HOPPEL HYPOTHESIS EXPERIMENTS, FOG LIQUID WATER CONTENT (g m^{-3})

Date	Daily Fog Number	Time (EST)	
10/30/90	1	1705	0.036
		1706	0.080
		1707	0.085
		1708	0.059
		1709	0.064
		1710	0.022
10/30/90	2	1800	0.009
		1801	0.101
		1802	0.095
		1803	0.069
		1804	0.050
		1805	0.009
10/30/90	3	1855	0.117
		1856	0.117
		1857	0.106
		1858	0.101
		1859	0.069
		1900	0.055
		1901	0.064
10/31/90	1	1513	0.031
		1514	0.142
		1515	0.108
		1516	0.089
		1517	0.065
10/31/90	2	1613	0.005
		1614	0.0128
		1615	0.235
		1616	0.186
10/31/90	3	1617	0.118
		1618	0.021
		1619	0.010
10/31/90	4	1826	0.003
		1827	0.184
		1828	0.223
		1829	0.123
		1830	0.116
		1831	0.028

Table 5
HOPPEL HYPOTHESIS EXPERIMENTS, FOG LIQUID WATER CONTENT (g m^{-3}) (cont.)

Date	Daily Fog Number	Time (EST)	
11/1/90	1	1551	0.178
		1551:30	0.220
		1552	0.198
		1553	0.171
		1554	0.154
		1555	0.139
		1556	0.004
11/1/90	2	1658	0.132
		1659	0.129
		1700	0.144
		1701	0.141
		1702	0.126
		1703	0.009
11/1/90	3	1848	0.002
		1849	0.153
		1850	0.153
		1851	0.126
		1852	0.108
		1853	0.014
		1854	0.004
11/2/90	1	1327	0.011
		1328	0.16
		1329	0.125
		1330	0.079
		1331	0.058
		1332	0.018
11/2/90	2	1507	0.111
		1508	0.088
		1509	0.084
		1510	0.093
11/2/90	3	1606	0.093
		1607	0.088
		1608	0.071
		1609	0.071
		1610	0.054

Table 5
HOPFEL HYPOTHESIS EXPERIMENTS, FOG LIQUID WATER CONTENT ($g\ m^{-3}$) (cont.)

Date	Daily Fog Number	Time (EST)	
11/2/90	4	1730	0.086
		1731	0.076
		1732	0.076
		1733	0.076
11/2/90	5	1823	0.024
		1824	0.147
		1825	0.120
		1826	0.105
		1827	0.076
		1828	0.024
11/3/90	1	1232	0.071
		1233	0.194
		1234	0.182
		1235	0.163
		1236	0.145
		1237	0.042
11/3/90	2	1328:30	0.114
		1329	0.232
		1330	0.181
		1331	0.165
		1332	0.150
		1333	0.135
11/3/90	3	1452	0.188
		1453	0.177
		1454	0.159
		1455	0.126
		1456	0.113
11/9/90	1	1322	0.113
		1323	0.180
		1324	0.166
		1325	0.140
		1326	0.120
		1327	0.110
11/9/90	2	1452	0.15
		1453	0.13
		1454	0.11
		1455	0.09
		1456	0.076

Table 5
HOPPEL HYPOTHESIS EXPERIMENTS, FOG LIQUID WATER CONTENT (g m^{-3}) (cont.)

Date	Daily Fog Number	Time (EST)	
11/9/90	1	1612	0.22
		1613	0.20
		1614	0.18
		1615	0.16
		1616	0.14
		1617	0.01
11/9/90	2	1928	0.005
		1929	0.14
		1929:30	0.151
		1930	0.138
		1931	0.114
		1932	0.080
		1933	0.064
11/9/90	3	2025	0.086
		2026	0.195
		2027	0.180
		2028	0.159
		2029	0.136
		2030	0.050
11/10/90	1	1234	0.11
		1235	0.15
		1236	0.14
		1237	0.13
		1238	0.04
11/10/90	2	1405	0.13
		1406	0.17
		1407	0.16
		1408	0.05
11/10/90	3	1443	0.22
		1444	0.21
		1445	0.20
		1446	0.18

Table 5
HOPPEL HYPOTHESIS EXPERIMENTS, FOG LIQUID WATER CONTENT (g m^{-3}) (cont.)

Date	Daily Fog Number	Time (EST)	
12/3/90	1	1535	0.01
		1536	0.11
		1537	0.22
		1538	0.19
		1539	0.18
		1540	0.17
		1541	0.14
		1542	0.13
		1543	0.02
12/3/90	2	1719	0.005
		1720	0.008
		1721	0.13
		1722	0.20
		1723	0.19
		1724	0.17
		1725	0.16
		1726	0.15
		1727	0.14
		1728	0.14
		1729	0.02
12/4/90	1	1607	0.03
		1608	0.15
		1609	0.13
		1610	0.11
		1611	0.08
		1612	0.06
		1613	0.03
12/5/90	1	1400	0.06
		1401	0.13
		1402	0.13
		1403	0.11
		1404	0.09
		1405	0.09
		1406	0.07

Table 5
HOPPEL HYPOTHESIS EXPERIMENTS, FOG LIQUID WATER CONTENT (g m^{-3}) (cont.)

Date	Daily Fog Number	Time (EST)	
12/5/90	2	1520	0.06
		1521	0.15
		1522	0.12
		1523	0.10
		1524	0.09
		1525	0.07
		1526	0.06
		1527	0.05
		1528	0.005
12/5/90	3	1722	0.03
		1723	0.14
		1724	0.15
		1725	0.13
		1726	0.10
		1727	0.08
		1728	0.08
		1729	0.05
		1730	0.04
		1731	0.02
		1732	0.02
12/6/90	1	1245	0.05
		1246	0.15
		1247	0.11
		1248	0.09
		1249	0.05

2.4 DMS PHOTOLYSIS EXPERIMENTS

2.4.1 Experimental Approach and Data Acquired

Experiment days for the photolysis investigations usually involved a single, relatively long-term experiment (6–10 hours), but on occasion, a day involved two experiments, between which the atmosphere from the first experiment was flushed from the chamber and replaced with fresh air for the second experiment. As with the Hoppel Hypothesis experiment days, the instruments were zeroed and the full-scale readings checked at the beginning of each experiment day.

Important to these experiments is the NO/NO_x concentration, since these species act as a catalyst for the reactions of DMS to MSA and SO_2. Because the concentrations being used were near the lower limit of the instrument, it was usually zeroed just before injection of NO into the chamber. Therefore, on a given experiment day, multiple zero offsets are provided for this instrument. Because of instrument drift, interpretation of measured time sequences of NO/NO_x in terms of experimental time histories is questionable. Zeroing the instrument just before injection of the species into the chamber, however, provided confidence in the measured input concentration

The experimental design was to study the photolysis of DMS and its resultant products, both gaseous and particulate. Two basic experiments were run. One type involved presetting the level of ozone by injecting it into the chamber prior to initiating UV irradiation; in the other type, the ozone formed as the irradiation proceeded. In both types, NO was added for catalytic purposes. In the experiments in which ozone was initially present, the injected NO immediately converted to NO_x. On the other hand, when no ozone was initially present, NO slowly converted to NO_x as the experiment generated O_3.

2.4.1.1 Experiment Logs

In the experiment logs, experiment days are numbered consecutively by calendar day. On a given day, data are provided for each test on that day. Table 6 shows the controlled inputs in terms of chemical constituents added to produce the chamber atmosphere in which chemical reactions occurred as well as whether UV irradiation took place. A plus sign and checkmark indicates that the species was added to the chamber atmosphere for the current test, while a checkmark alone indicates a species was probably still present from preceding tests. The presence of ion chromatograph data is indicated, as well as comments where warranted.

Table 6
LOG OF DMS PHOTOLYSIS EXPERIMENTS

			INPUTS							
Experiment Day	Date	Test	DMS	O_3	H_2O_2	NO	UV	SO_2	Ion Data	Comments
1	11/5	1					√			
		2		⊕√						
		3		√				⊕√		
		4		√			√	⊕√		
		5		√		⊕√ (NO_2)				
		6		√		√	√			k_d Computations
2	11/6	0	⊕√							
		1	⊕√				√		√	
	Filtered									
		2	⊕√	⊕√						Dark Reaction Rate Check
		3	√				√			
		4	√	√						
		5	√	√			⊕√ (H_20)			
		6	√	√	⊕√		√ (H_20)			
3	11/7	1	⊕√	⊕√			√		√	
		2	√	√		⊕√	√			
		3	√	√		⊕√	√		√	

√ Probably present from previous test
⊕√ Added for current test.

Table 6
LOG OF DMS PHOTOLYSIS EXPERIMENTS (cont.)

			INPUTS							
Experiment Day	Date	Test	DMS	O_3	H_2O_2	NO	UV	SO_2	Ion Data	Comments
4	11/8	1	⊕√	⊕√		⊕√				
	Filtered									
		2	⊕√			⊕√			√	Literature Results Test
5	11/26	1	⊕√				√			Pre-test Filtered
	Filtered									
		2	⊕√	⊕√			√			Pre-test Filtered
		3	√	√		⊕√				DMS & O_3 from Test 2
		4	√	√		⊕√	√		√	
6	11/27	1		⊕√						
		2	⊕√	√		⊕√			√	

√ Probably present from previous test
⊕√ Added for current test.

Table 6
LOG OF DMS PHOTOLYSIS EXPERIMENTS (cont.)

			INPUTS							
Experiment Day	Date	Test	DMS	O_3	Propylene	NO	UV	SO_2	Ion Data	Comments
7	11/28	1		⊕√						Complex set of exps. since no filtering between tests
		2		√			√			
		3	⊕√	√						
		4	√	√			√			
		5	√	√	⊕√					
		6	√	√	√		√			
		7	√	⊕√	√	⊕√			√	
		8	√	⊕√	√	√	√			
		9	√	√	√	⊕√	√		√	
8	11/29	1	⊕√	⊕√	⊕√					Discovered oil leak on mixing fan motor
		2	√	⊕√	√		√			Motor sealed in Teflon Bag.
		3	√	√	√	⊕√			√	Again complex set of tests.
		4	√	⊕√	√	√	√			
		5	√	√	√	⊕√	√		√	Ion Data Background
		6	⊕√	√	√	√	√			
		7	√	√	√	⊕√	√		√	
		8	√	√	√	√	√	⊕√	√	NH_3 added

√ Probably present from previous test
⊕√ Added for current test.

Table 6
LOG OF DMS PHOTOLYSIS EXPERIMENTS (cont.)

			INPUTS						
Experiment Day	Date	Test	DMS	O_3	NO	NH_3	UV	Ion Data	Comments
9	11/30	1	⊕√	⊕√	⊕√			√	
		2	√	√	√		√		
		3	√	√	⊕√		√		
		4	√	√	√		√	√	Increase RH
		5	√	⊕√	√		√	√	
		6	√	√	√	⊕√	√	√	
10	12/1	0						√	Ion data clean chamber
		1	⊕√		⊕√		√	√	"Classic" Smog Experiment performed by others and reported on in literature.

√ Probably present from previous test
⊕√ Added for current test.

2.4.1.2 *Zero Offsets*

Tables 7 and 8 show the zero offsets for the various gas instruments. At the beginning of each experimental day, zero readings were checked for each instrument. In addition, periodic span checks were performed using known gas concentrations. The instruments listed in Table 7 were stable and the zero offset is listed only for the beginning of each experimental day. On the other hand, the NO/NO_x instrument (Table 8) suffered from signal drift and it was zeroed just before an injection of NO into the chamber. Thus measurement of the injected amount of NO is reasonable, but confidence in the measurement declines directly with elapsed time into the experiment after setting the zero.

2.4.1.3 *Aerosol Chemical Analyses*

Table 9 shows the chemical composition of the aerosol which existed at times during the DMS photolysis experiments. The aerosol was collected on a filter which was usually exposed for approximately 8–10 minutes at a nominal flow rate of 30 cubic feet/min. The collected aerosol was then washed from the filter with dionized water, and the solution injected into an ion chromatograph from which the concentrations of the various ions reported in Table 9 were obtained.

Table 7
DMS PHOTOLYSIS EXPERIMENTS, INSTRUMENT ZERO OFFSETS

Date	Time	Total Sulfur (ppb)	SO_2 (ppb)	O_3 (ppm)
11/5/90	1105	1.0	1.5	+.001
11/6	0905	4.0	1.5	+.001
11/7	0833	4.0	1.3	+.001
11/7	1435	-3.2	1.3	+.001
11/7	1632	0.4	1.3	+.001
11/8	0953	4.0	1.4	+.001
11/26	0950	4.0	1.3	+.001
11/27	0930	4.0	1.3	+.001
11/28	0946	3.5	1.5	+.001
11/29	1132	4.0	1.3	+.001
11/30	0909	6.0	1.3	+.001
12/1	1036	5.0	1.1	+.001

Table 8
DMS PHOTOLYSIS EXPERIMENTS, NO_x AND NO OFFSETS

Date	Time	Zero Offset	
		NO_x (ppm)	NO(ppm)
11/5/90	1832	−.004	−.005
11/6	0955	+.0006	+.0013
11/6	1547	+.001	+.0008
11/7	1012	−.0019	−.0098
11/7	1435	−.0016	−.0030
11/7	1630	−.0003	−.0005
11/8	1046	+.0018	+.0024
11/8	1058	+.0036	+.0041
11/8	1106	+.0044	+.0038
11/8	1451	−.0004	+.0008
11/26	1038	−.0005	−.0007
11/26	1340	−.010	−.010
11/26	1624	±.000	+.0006
11/27	1337	+.0017	−.0005
11/27	1424	+.0037	−.0031
11/28	0941	+.017	+.017
11/28	1555	+.024	+.024
11/28	1825	+.007	+.003
11/28	1842	+.0018	+.0022
11/29	1130	+.011	+.0112
11/29	1431	+.0134	+.016
11/29	1636	+.0115	+.011
11/29	1840	+.019	+.0125
11/30	1013	+.0176	+.020
11/30	1231	+.021	+.0187
12/1	1037	+.018	+.020
12/1	1127	+.0186	+.0206

Table 9
CHEMICAL CONSTITUENTS FOR DMS PHOTOLYSIS EXPERIMENTS

Sample No.	Date	Time	Volume Sampled (m^3)	MSA ($\mu g/m^3$)	SO_4 ($\mu g/m^3$)	NO_3 ($\mu g/m^3$)	NH_3 ($\mu g/m^3$)	
22	11/6	1306-1406	54.0	<0.04	0.9	0.3	-	
23	11/7	1258-1403	57.4	<0.04	0.65	0.3	-	
24	11/7	1813-1913	54.0	0.83	0.95	0.6	-	
25	11/8	1910-1940	25.0	1.03	0.60	0.46	-	
34	11/26	1818-1828	10.3	0.44	3.09	1.38		
35	11/27	1644-1654	10	2.47	3.7	2.5		
36	11/28	1712-1717	5	<0.2	2.101	.13		
37	11/28	1946-1956	9.8	1.1	1.41	2.11		
38	11/29	1542-1547	4.66	0.19	4.68	<0.1		
39	11/29	1547	20 sec Background	<0.05	<1	<0.5	Total in Filter	
40	11/29	1921-1926	4.66	1.38	1.39	4.7		
41	11/29	2003-2008	5.13	1.64	1.04	4.3		
42	11/30	1147-1152	4.66	0.34	1.52	4.61		
43	11/30	1448-1453	4.66	1.03	1.46	4.61		
44	11/30	1606-1611	4.66	1.48	1.37	4.38		
45	11/30	1729-1739	9.4	2.09	0.76	2.46		
46	12/1	0857-0933	33.6	0.45	0.09	0.187	Clean Chamber	
47	12/1	1536-1546	9.4	1.77	0.76	2.27		

2.4.2 UV Light Intensity

2.4.2.1 Measurement of UV Spectrum

In 1990, prior to this set of experiments, the ultraviolet irradiation system was refurbished by replacing both the fluorescent lights and black lamps. Subsequent to the 1990 experiments, measurements were made of the spectral irradiance in the chamber using an EG&G Optical Multichannel Analyzer (OMA). Figure 7 shows a relative spectral response for the irradiance as averaged from about one-third of the chamber circumference, thereby including a number of lamp column housings and large expanses of wall surfaces. The spectrum shows a peak irradiance at 350 nm and half power points at ±20 nm. Atomic mercury lines are superimposed at 365 and 406 nm.

A tungsten filament standard lamp was used to calibrate the system in terms of relative spectral response. Several other measurements were made to establish the spectral output of the chamber lamps, as well as that of the wall itself when illuminated by the lamps. These data indicate that the walls are spectrally neutral; they do not alter the spectrum of the incident radiation.

2.4.2.2 Measurement of k_1

The chamber light intensity as monitored by photodissociation of NO_2 in air gave a $k_1 = \left(\frac{d\ [O_3]}{[NO_2]_o\ dt} \right)_{t=0}$ (Wu and Niki, 1975) of 0.39 min^{-1}. This value compares to k_1 = 0.325 min^{-1}, with a probable error of ±15%, computed from the photostationary state of [NO], [O_3] and [NO_2] (ibid.).

2.4.3 Long Term Experiments

During the experimental period, two, long term, overnight experiments were run. The first one (Figure 8) shows decay of SO_2 when the chamber volume was sealed and isolated and the interior mixing fan was on. The second experiment (Figure 9) was a long term DMS photolysis in which ozone at 300 ppb and DMS were irradiated by the UV light system.

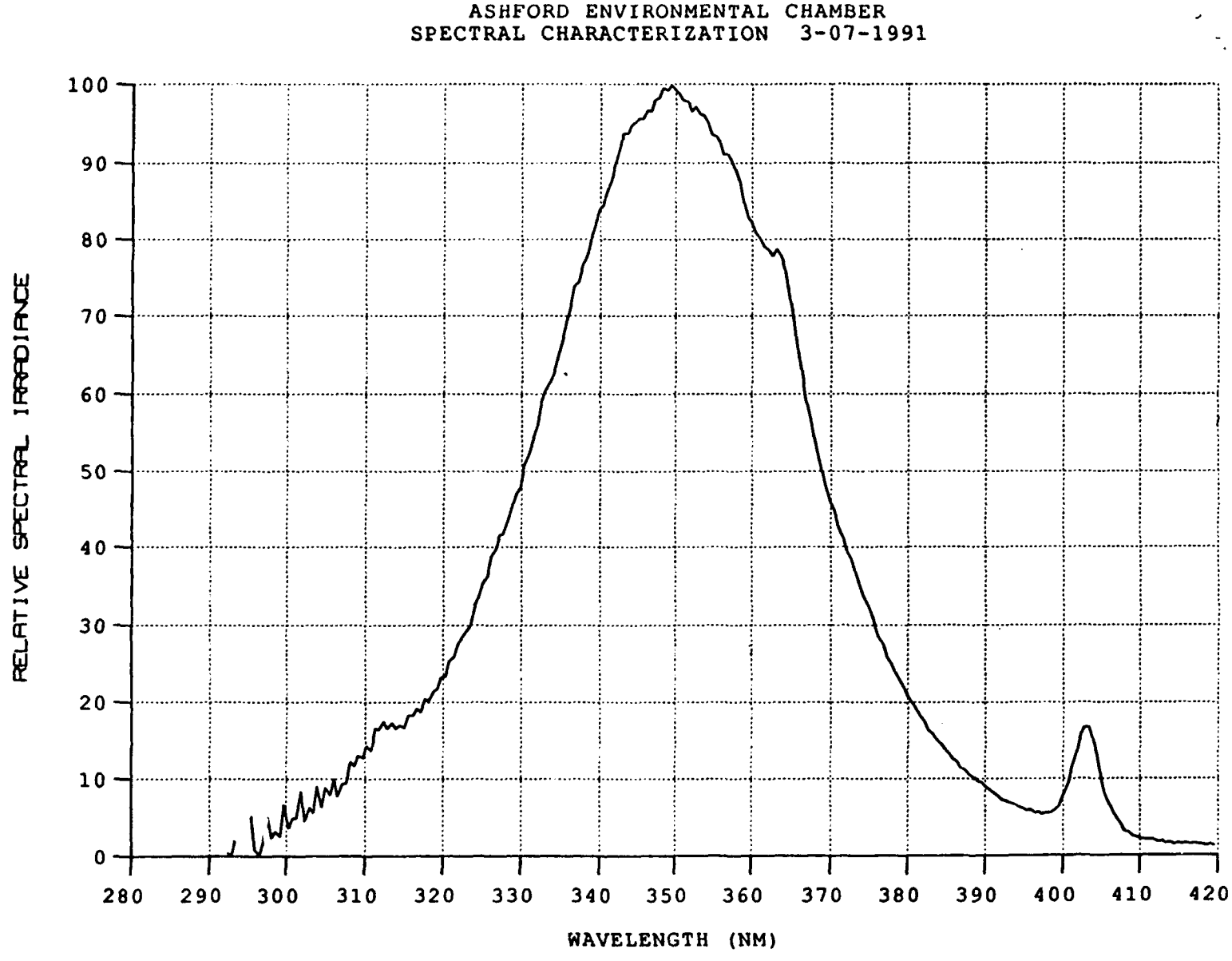

Figure 7 ASHFORD ENVIRONMENTAL CHAMBER SPECTRAL CHARACTERIZATION

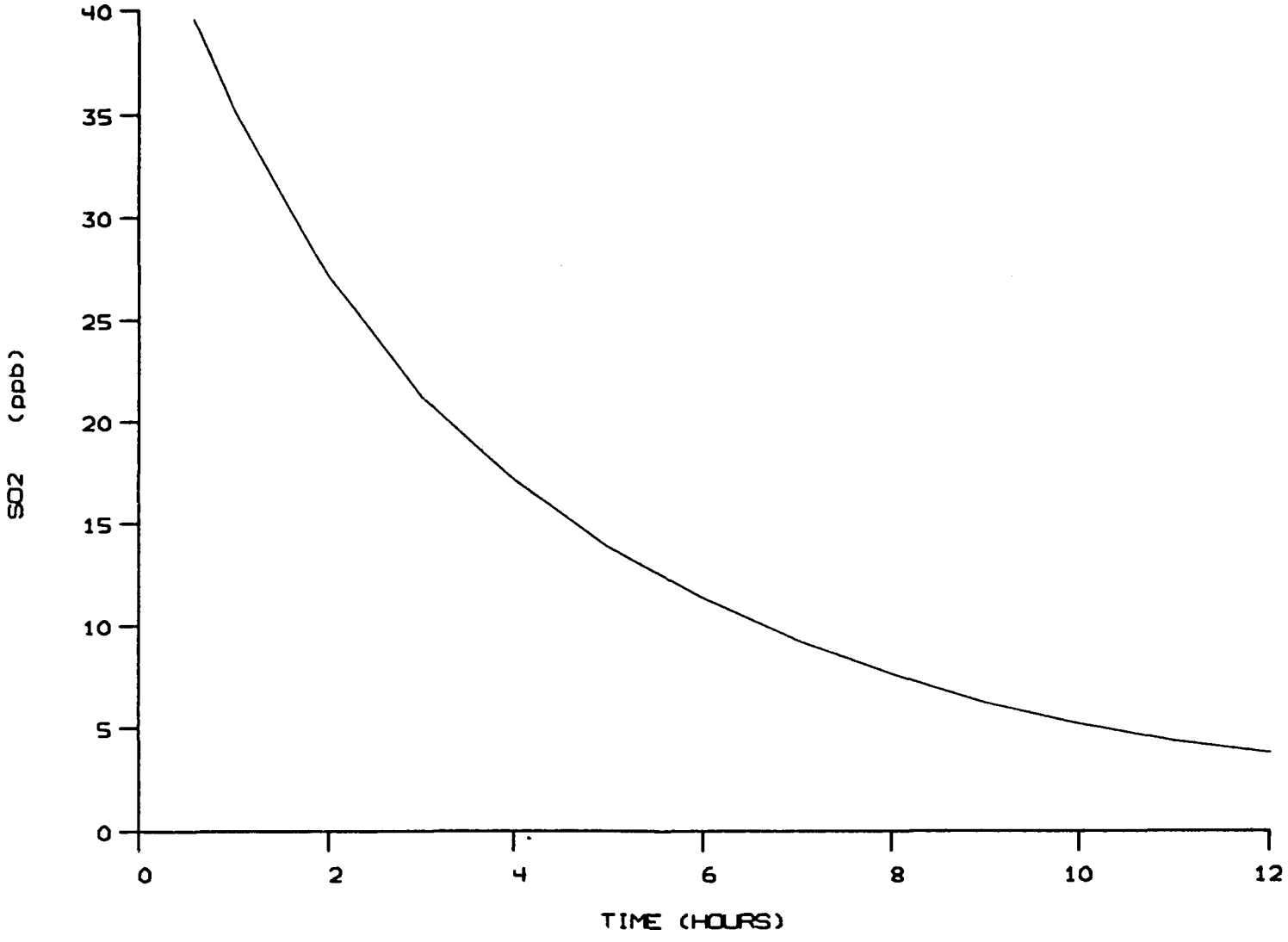

Figure 8 SO_2 DECAY

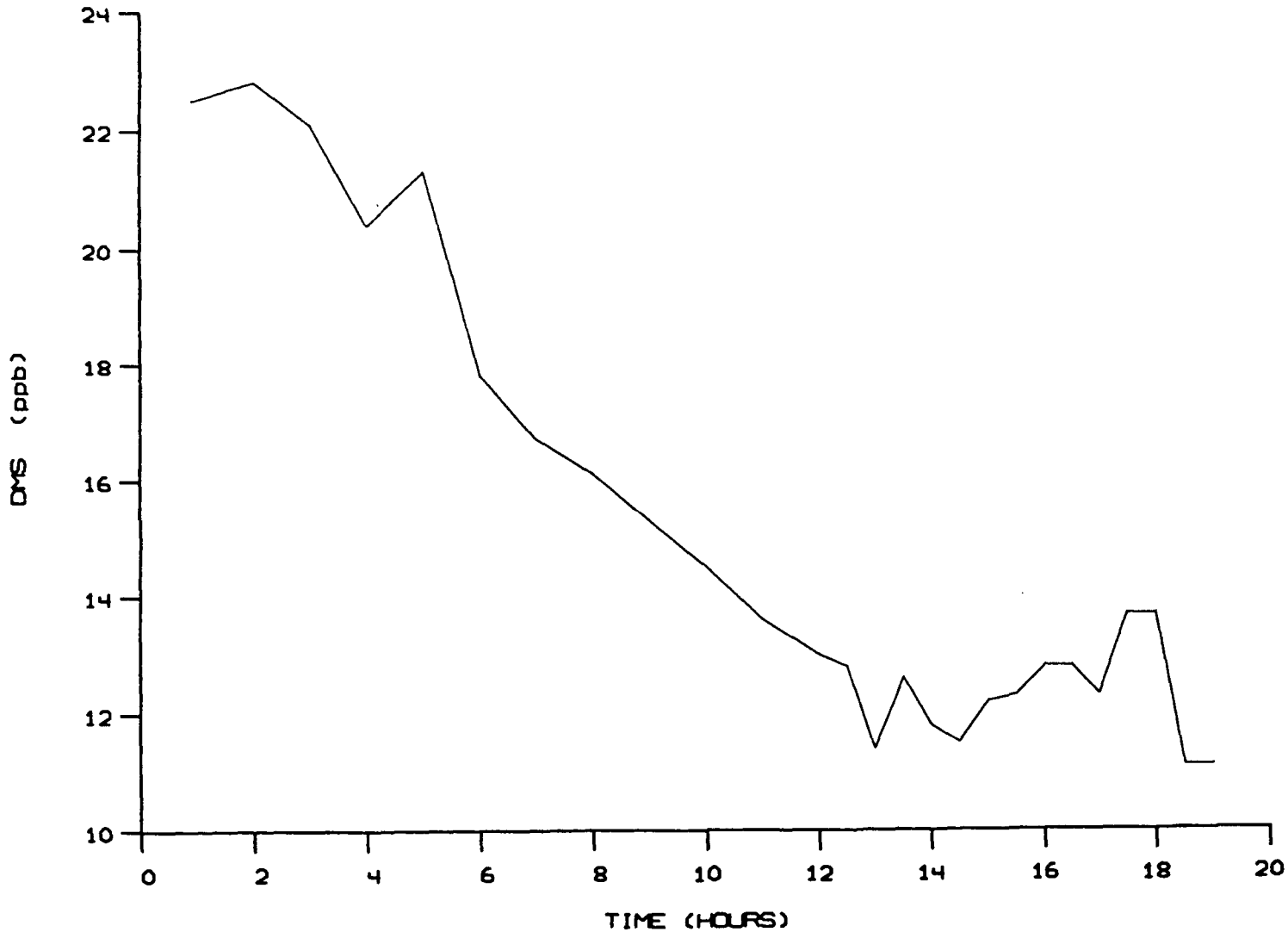

Figure 9 DMS PHOTOLYSIS

2.4.4 Summary of Photolysis Results

This section presents a qualitative summary of results of the photolysis experiments, obtained after an initial "quick-look" at the data. More detailed analysis will be required to quantify photolysis rates and product branching ratios. Table 10 provides a tabular summary of each experiment day for the photolysis experiments. The time is listed first (indicating a separate experiment) as well as the purpose, constituents in the chamber and results.* The table provides a summary of the results in the context of the history of each day's experiments. This context is important since the chamber was usually not flushed with clean air between experiments (i.e., reactants were added in a step-wise fashion). However, for the qualitative summary presented below, the results will be presented in terms of reactant combinations. The experiment dates are shown in parentheses.

1. *Background Non-Methane Hydrocarbon (NMHC).* (11/5) The "clean" chamber (rural environment) was found to typically contain 70–130 ppb of NMHC. Unless otherwise noted, this background level can be assumed to be present in the experiments discussed below. Typical background levels of MSA, sulfate and nitrate (as measured via ion chromatograph), were 0.04, 0.09 and 0.19 $\mu g/m^3$ respectively. A small increase, 3000/cc (3K), in condensation nuclei (CN) was observed when the UV lights were turned on.

2. *O_3.* (11/5, 11/7, 11/27) When O_3 was added to the clean chamber at levels of 100–350 ppb, no significant reaction [as evidenced by an increase in condensation nuclei(CN)] was observed under dark conditions. Later experiments with 500 ppb O_3 in a dark chamber (with DMS) also showed no measurable activity. However, significant activity was observed in the dark chamber at high concentrations of O_3 (1000 ppb) in a clean chamber (NMHC = 80 ppb). Thus it appears some threshold between 500 and 1000 ppb may be required before measurable activity is observed in the dark. When low levels of O_3 (340 ppb) were irradiated causing the photolytic dissociation of O_3, generation of CN occurred.

3. *O_3 + SO_2.* (11/5) When SO_2 (1–4 ppb) was entered into the chamber along with O_3 (140 ppb) very little increase in CN was noted during dark periods. However, when the lights were turned on, CN levels increased to as high as 55K suggesting O_3 photolysis with subsequent formation of OH then reacted with the SO_2 to eventually form sulfate. The size distribution continued to grow for about 10–20 minutes after the lights were turned off

* This tabulation was initially compiled by Dr. Hoppel et al., with additional ion chromatograph data provided by Calspan

4. *DMS.* (11/6, 11/26) Small amounts (35 ppb) of DMS in the chamber (with NMHC at 80 ppb) produced essentially no reaction in the dark. Upon irradiation, O_3 was produced as well as SO_2. CN levels increased to 30K. The ion chromatograph (IC) data indicated some sulfate was formed but no measurable methane sulfonic acid (MSA). When slightly higher levels of DMS were added (50 ppb) and irradiated (11/26) in the presence of lower levels of NMHC (40 ppb), significantly higher levels of CN were produced (102K, decreasing to 87K) although lower levels of O_3 and SO_2 were obtained.

5. *DMS + O_3.* (11/6, 11/7, 11/26) When O_3 (120 ppb) was added to DMS (35 ppb) in the dark (11/6), nothing happened. Similar results were obtained (11/7) when higher concentrations of DMS (50 ppb) and O_3 (490 ppb) were used, i.e., no reaction in the dark. When irradiated (11/6), the photolysis rate was low (small increase in CN, little SO_2 produced), however, this may have been due to interference from the high concentrations of NMHC (500 ppb) present at the time. Some increase in photolysis was noted on (11/7) when higher amounts of reactants were used (but also the NMHC concentration was lower). On 11/26, when larger amounts of O_3 (1000 ppb) were added to DMS (50 ppb), in the presence of low NMHC (130 ppb), significant conversion took place in the dark with CN levels changing from 31K to 127K to70K and SO_2 increasing. When the lights were turned on, continued gas to particle conversion occurred but no new CN were created.

6. *NO.* (11/8) The addition of NO to the chamber with NMHC (1950 ppb) showed no particle formation in either the dark or when irradiated. Small amounts of SO_2 were produced in the dark (residual S compounds?).

7. *DMS + NO.* (11/8, 11/27) When DMS (40 ppb) was combined with NO (20 ppb) in a dark chamber (NMHC = 1950 ppb) no measurable conversion occurred. When similar concentrations (NO = 30 ppb) were irradiated (11/27), CN increased from 30 to 200K (about 10 minutes after lights were turned on). A significant amount of SO_2 was formed (2.5 ppb) as well as O_3 (114 ppb product). The IC data (11/27) showed MSA = 2.47 $\mu g/m^3$, SO_4 = 3.7 $\mu g/m^3$ and NO_3 = 2.5 $\mu g/m^3$. Lower amounts were observed at lower concentrations of NO (11/8). The concentration of NMHC was high on both days. The IC data are higher than that obtained when ozone is included as a reactant with NO (cf. 8. following).

8. *DMS + O_3 + NO.* (11/7, 11/8, 11/26) DMS (40 ppb) with O_3 (120 ppb) and NO (20 ppb) *in the dark* (11/8) showed a significant conversion of gas to particle with a CN count increasing from 32 to 80K. Some SO_2 product was formed (0.4 ppb). There was a large background of NMHC

during this time (1100 ppb). However, a second experiment (11/26) with lower NMHC (117 ppb) but higher O_3 (793 ppb), also showed significant reaction in the dark (SO_2 product increasing from 1 to 3 ppb). When irradiated (11/7), DMS (less than 50 ppb) + O_3 (250 ppb) + NO (10 ppb) in the presence of 216 ppb of NMHC, showed an increase of CN from 22K to a maximum of 86K and an SO_2 increase from 1.6 to 2.7 ppb. Increasing the NO to 30 ppb resulted in a very large conversion (CN = 289K, SO_2 increased to 4.8 ppb). MSA, SO_4 and NO_3 all exceeded background levels (although all were less than 1 $\mu g/m^3$. However, these samples were taken after the CN count had decreased from the maximum). When O_3 was increased to approximately 660 ppb (11/26) and irradiated, both SO_4 and NO_3 increased significantly to 3.09 and 1.38 $\mu g/m^3$ respectively, while MSA decreased (0.44 $\mu g/m^3$). These levels were still below that observed with only NO and no O_3 added to the DMS, with the largest difference occurring for MSA.

9. *DMS + O_3 + C_3H_6* (11/28, 11/29) Large numbers of particles were formed in the dark (11/29) when DMS (50 ppb), O_3 (300 ppb) and C_3H_6 (200–380 ppb) were entered into the chamber with NMHC = 450 ppb. O_3 decreased rapidly when C_3H_6 was added. No significant increase in particles was observed when the lights were turned on.

10. *DMS + O_3 + C_3H_6 + NO.* (11/28, 11/28) When DMS (50 ppb), O_3 (280 ppb) and C_3H_6 (400 ppb) were combined with 20 ppb of NO in the dark, the CN increased from 38K to 180K with an increase in SO_2 of more than 2 ppb (11/29) (NMHC = 1000 ppb). With respect to IC data, the major product in the dark was SO_4 whose concentration increased with increasing levels of O_3 and C_3H_6. When illuminated, a significant increase of MSA and NO_3 occurred relative to the dark reaction, while SO_4 decreased. Again, increased products were found when the concentrations of O_3 and C_3H_6 increased.

11. *DMS + O_3 + NO + NH_3.* (11/29, 11/30) NH_3 (20 ppb) was added in the presence of DMS (50 ppb), O_3 (200 ppb) and NO (30–35 ppb). (Some amount of propene may also have remained in the chamber from earlier in the day.) Upon irradiation, SO_2 increased slightly and MSA increased from 1.38 to 1.64 $\mu g/m^3$. A decrease in both NO_3 and SO_4 was observed

12. *DMS + H_2O_2 + O_3.* (11/26) When irradiated, CN increased from 6.5 to 38K and the size distribution grew rapidly (NMHC = 900 ppb).

In summary, reactions occurred in the dark under conditions of high ozone concentrations (1000 ppb). Adding NO seemed to lower the threshold for dark reactions [i.e., lower ozone concentration (120 ppb)] was required in the presence of NO to initiate reactions with DMS in the dark (no experiments were

performed with only NO and ozone]. NO alone with DMS showed no reaction in the dark. Reactions occurred in the dark with NO + O_3 + DMS with and without high concentrations of NMHC. DMS + O_3 + C_3H_6 showed significant reaction in the dark (i.e., large numbers of particles formed, rapid decrease in O_3, but this is not surprising since C_3H_6 reacts readily with O_3). Adding NO to this mixture appeared to produce increased SO_4 and SO_2 products in the dark. No experiments were performed with addition of NH_3 in the dark.

Photolysis of DMS with no added oxidizer produced O_3 and SO_2 products as well as increased CN (sulfate). Adding O_3 to DMS resulted in an apparent lower photooxidation rate, however, this may have been due to the presence of high NMHC in these particular experiments which could be scavenging the OH generated from ozone photolysis. Upon irradiation, DMS + NO showed a large increase in CN with significant products (SO_2, O_3, MSA, SO_4 and NO_3). DMS + NO + O_3 shows large production of CN and SO_2 although the IC data were noticeably below that observed for similar concentrations of DMS and NO without O_3. Adding an excess of O_3 resulted in increased SO_4 and NO_3 but decreased MSA. For the DMS + NO + O_3 + C_3H_6 system, a significant increase in MSA and NO_3 occurred when illuminated while SO_4 decreased (relative to the dark reaction). A few experiments, in which NH_3 was added to the chamber in the presence of DMS, O_3 and NO, showed decreases in SO_4 and NO_3 but an increase in MSA.

The results just summarized are at best preliminary. Careful examination of wall losses, time of IC data samples relative to the addition of reactants, rate of increase of various products (as opposed to maximum amount) etc., must be considered in a detailed analysis. Future work should include the addition of a mass spectrometer to identify and monitor trace species, NMHC, etc.

Table 10
NRL SUMMARY OF DMS PHOTOLYSIS EXPERIMENTS

TIME	PURPOSE	CONSTITUENTS IN CHAMBER	RESULTS
5 November 1990			
1140-1320	Background aerosol formation in clean chamber	Clean - 70 ppb NMHC Lights on 1140-1304	- CN increased 0 --> 3000/cc - Did not grow into DMA range
1420-1530	Background aerosol formation with O_3 Dark chamber	$O_3 \approx$ 150 ppb (added @ 1430)	- CN increased 80 --> 170/cc - No particles in DMA range
1531-1555	Aerosol formation with O_3 and SO_2 Dark chamber	NMHC = 100-120 ppb SO_2 = 0.2 ppb O_3 = 140 ppb	-CN increased 170 --> 1300/cc - Insignificant increase in DMA
1600-1640	See is photolysis of O_3 to OH increased formation rate	Lights on at 1607 SO_2 = 0.8 ppb $O_3 \approx$ 130 ppb NMHC = 120-130 ppb	- CN increased from 4K --> 25K/cc - Particles appeared in DMA at about 1625
1645-1730	Increased SO_2 to get measurable photolysis rate	At 1645 SO_2 --> 2.6 ppb O_3 = 108 ppb NMHC = 140 ppb	CN increased to 55K/cc SO_2 dropped from 4.1 --> 2.4 ppb O_3 dropped 108 --> 95 ppb DMA S.D. grew
1730-1800	See if S.D.* stopped growing when lights are turned off	Lights off 1730-->1800	S.D. did not stop growing for 10-20 minutes after lights were turned off
1800-1830	See if S.D. growth resumed when lights were turned back on	1800 lights turned on SO_2 = 1.7 ppb O_3 = 84 ppb	

* S.D. = Aerosol Size Distribution from the NRL Differential Mobility Analyzer

Table 10
NRL SUMMARY OF DMS PHOTOLYSIS EXPERIMENTS (cont.)

TIME	PURPOSE	CONSTITUENTS IN CHAMBER	RESULTS
6 November 1990 0955-1120	DMS + DARK CLEAN CHAMBER	NMHC ≈ 80 ppb O_3 = 0 DMS = 6 ppb	Nothing happened CN 1 --> 20/cc
1121-1305	DMS + LIGHTS CLEAN CHAMBER (added 35 ppb to get TS reading)	T.S. = 36 mv* 1146 - Turn lights on 1303 - Lights off	CN increased 34 --> 30K/cc O_3 increased 1 --> 7.8 ppb SO_2 increased 0.5 --> 1.8 ppb
IC 1306-1406 CHAMBER FILTERED			SO_4 = 0.9 $\mu g/m^3$ MSA = <0.04 $\mu g/m^3$ NO_3 = 0.3 $\mu g/m^3$
1545-1640	DMS and O_3 + DARK At 1550 add 40 ppb DMS At 1603 add 120 ppb O_3	NMHC ≈ 500 ppb (increased during filtering) T.S. = 37 mv O_3 = 115 ppb	CN = 25 --> 39/cc
1640-1900	DMS + O_3 + LIGHTS	1640-1815 Lights on NMHC = 490 ppb O_3 = 107 ppb T.S. = 37.3 mv SO_2 = 0.3 ppb Lights off 1816-1836 on 1836-1900	CN increased 39 --> 4730/cc SO_2 increased 1.7 --> 2.2 ppb O_3 decreased 107 --> 78 ppb Particles appeared in DMA @ 1830
1931-2046	DMS and H_2O_2 Add H_2O_2 with lights on photolysis of H_2O_2 --> 20H	NMHC = 900 ppb O_3 = 60 ppb T.S. = 35.7 mv SO_2 = 1.4 ppb	CN increased 6.5K --> 38K DMA - S.D. grew rapidly

* T.S.= Total Sulfur in units of millivolts, see Fig. 6 for calibration.

Table 10
NRL SUMMARY OF DMS PHOTOLYSIS EXPERIMENTS (cont.)

TIME	PURPOSE	CONSTITUENTS IN CHAMBER	RESULTS
7 November 1990			
1010-1050	DMS + O_3 + DARK Add DMS @ 1013 (50 ppb) Add O_3 @ 1034 (500 ppb)	T.S. = 40 mv O_3 = 490 ppb NMHC = 100 ppb	Nothing in 40 min.
1050-1300	DMS + O_3 + LIGHTS	Lights on @ 1054 T.S. = 40.5 mv O_3 = 480 ppb NMHC = 120 ppb RH = 45%	CN 13 --> 50K/cc SO_2 increased 0.5 --> 2.0 ppb O_3 decreased 487 --> 359 ppb Particles in DMA @ ~1130
IC 1258-1403			SO_4 = 0.65 $\mu g/m^3$ MSA = <0.04 $\mu g/m^3$ NO_3 = 0.3 $\mu g/m^3$
1430-1630	DMS + O_3 + NO + LIGHTS Add 10 ppb NO @ 1434	T.S. = 34.9 mv O_3 = 250 ppb NMHC = 216 ppb SO_2 = 1.6 ppb	Big increase CN 22.1K --> 35K MAX CN = 86K O_3 = 250-->189 ppb with intermediate maximum SO_2 = 1.6 --> 2.7 ppb
1630-1805	DMS + O_3 + NO + LIGHTS Increase NO enough to get reading Add 30 ppb NO @ 1631	T.S. = 30.9 --> 25.4 mv O_3 = 169 --> 190 --> 189 ppb NMHC = 330-400 ppb NO_x = 10 ppb SO_2 = 2.8 --> 4.8 ppb	CN = 51K --> 289K --> 68.7K SO_2 = 2.8 --> 4.8 ppb Very large conversion rate
IC 1813-1913			SO_4 = 0.95 $\mu g/m^3$ MSA = 0.83$\mu g/m^3$ NO_3 = 0.6 $\mu g/m^3$

Table 10
NRL SUMMARY OF DMS PHOTOLYSIS EXPERIMENTS (cont.)

TIME	PURPOSE	CONSTITUENTS IN CHAMBER	RESULTS
8 November 1990			
1045-1225 CHAMBER FILTERED	$DMS + O_3 + NO$ + DARK [Background NMHC is high] 1045 add 40 ppb DMS 1059 add 120 ppb O_3 1105 add 20 ppb NO	CN = 32 SO_2 = 0 NMHC = 1100 ppb T.S. = 33.2 mv O_3 = 113 ppb NO_x = 28 ppb	CN = 32 --> 80K/cc SO_2 = 0 --> 0.4 ppb T.S. = 33.2 --> 33.5 --> 33.3 mv O_3 = 113-69 ppb (Large Conversion rate in dark chamber) 1120 particles in DMA
1450-1520	NO + NMHC + DARK [NMHC is high background] 1452 add 20 ppb NO	CN = 25/cc SO_2 = 0 O_3 = 0 NO_x ≈ 20 ppb NMHC = 1950 ppb	No particle formation slight increase in SO_2 SO_2= 0 --> 0.5 ppb
1520-1540	NO + NMHC + LIGHTS 1520 - Lights ON 1536 - Lights OFF	NMHC CN = 28/cc SO_2 = 0.5 ppb NO_x ≈ 20 ppb	No particle formation (or SO_2 produced)
1545-1605	NO + NMHC + DMS + DARK 1545 Add 40 ppb DMS	NO_x ≈ 20 ppb CN = 36/cc SO_2 = 0.4 ppb T.S. = 34.3 mv O_3 = 0	No particle formation (or SO_2 produced) some NO_x was used up
1605-1900	NO + NMHC + DMS + LIGHTS 1605 - Lights ON	CN = 48/cc NO_x = 12 ppb O_3 ≈ 0 SO_2 ≈ 0.5 ppb NMHC = 2080 ppb	CN = 48 --> 256K --> 45K/cc SO_2 = 0.4 --> 2.4 ppb T.S. 33.6 --> 31.0 mv O_3 = 1 --> 120 ppb NO_x = 15 ppb --> <5 ppb At 1615 particles in DMA Very Large Conversion Rates
1910-1940 IC			SO_4 = 0.60 $\mu g/m^3$ MSA = 1.03 $\mu g/m^3$ NO_3 = 0.46 $\mu g/m^3$

Table 10
NRL SUMMARY OF DMS PHOTOLYSIS EXPERIMENTS (cont.)

TIME	PURPOSE	CONSTITUENTS IN CHAMBER	RESULTS
26 November 1990			
1035-1130	DMS - DARK Add 50 ppb DMS @ 1038	CN = 16/cc SO_2= 0 T.S. = 42 mv O_3 = 0 NMHC = 50 ppb	No particle formation
1130-1235 CHAMBER FILTERED	DMS - LIGHTS ON Lights on @ 1130	CN = 28 --> 102K --> 87K/cc SO2 = 0.2 -->. 0.4 ppb T.S. 44.8 mv (no change) O_3 1 --> 4 ppb NMHC ≈ 40 ppb	Large conversion rate 1150 particles appeared in DMA
1400-1520	DMS + O_3 + DARK 1400 Add 50 ppb DMS 1405 add 1000 ppb O_3	CN = 2830/cc (start) SO_2 ≈ 0 T.S. = 36.8 mv O_3 = 1002 ppb NMHC = 132 ppb	CN = 2800 --> 127K --> 70K/cc SO_2 = 0.1 --> 0.9 ppb --> Then remained constant T.S. = 36.7 mv constant O_3 = 1002 --> 918 ppb NMHC = 132 --> 105 ppb steady decrease
1520-1610	DMS + O_3 + LIGHTS ON 1520 Lights ON 1610 Lights OFF	CN = 70K/cc SO_2 = 0.7 ppb T.S. = 36.8 mv O_3 = 918 ppb NMHC = 105 ppb	Continued conversion but no new CN T.S. = 36.4 --> 35.6 mv
1620-1720	DMS + O_3 + NO + DARK 1624 add 10 ppb NO 1636 add 10 ppb NO 1704 add 6 ppb NO	CN = 42.1K/cc T.S. = 35.4 mv O_3 = 793 ppb NMHC = 117 ppb	Very large conversion rate SO_2 = 1 --> 3 ppb O_3 = 793 --> 680 ppb T.S. = 35.5 --> 26.6 mv New peak at 1640 coming in DMA
1720-1820	DMS + O_3 + NO + LIGHTS 1720 add 6.6 ppb NO 1721 LIGHTS ON	CN = 75.4 K SO_2 = 3.2 ppb O_3 = 663 ppb T.S. 26.2 mv NMHC ≈ 100 ppb	Continued large conversion rate Another new peak in DMA SO_2 = 3.2 --> 3.5 --> 3.0 ppb O_3 = 663 --> 583 ppb T.S. = 26.2 --> 20.5 mv
1818-1828 IC			SO_4= 3.09 $\mu g/m^3$ MSA = 0.44 $\mu g/m^3$ NO_3 = 1.38 $\mu g/m^3$

Table 10
NRL SUMMARY OF DMS PHOTOLYSIS EXPERIMENTS (cont.)

TIME	PURPOSE	CONSTITUENTS IN CHAMBER	RESULTS
27 November 1990 0930-1050 CHAMBER FILTERED	Background particle generation with high O_3	Filtered overnight NMHC 80 ppb Add 1000 ppb O_3 @ 0930	CN increase from 12 --> 47,000/cc
1300-1345	Background for DMS Photolysis experiment	NMHC increased during filtering to 1500 ppb Add ~45 ppb DMS @ 1308 1340 add ~30 ppb NO	
1345-1645	Photolysis of DMS with NO	Lights on at 1345 T.S. ≈ 45 mv $O_3 \approx 0$ $NO_x \approx 30$ ppb	CN increased from 30 to 200 K/cc First appeared in about 10 min after light was turned on
		Additional 10 ppb NO added at 1425	O_3 increased throughout run to 114 ppb SO_2 increased to ~2.5 ppb
IC 1644-1654			$SO_4 = 3.7\ \mu g/m^3$ $MSA = 2.47\ \mu g/m^3$ $NO_3 = 2.5\ \mu g/m^3$

Table 10
NRL SUMMARY OF DMS PHOTOLYSIS EXPERIMENTS (cont.)

TIME	PURPOSE	CONSTITUENTS IN CHAMBER	RESULTS
28 November 1990 0950-1140	Chamber background with O_3 - DARK Then with lights on	Filtered all night NMHC = 50 ppb Add ~150 ppb O_3 @ 0957 Add ~150 ppb O_3 @ 1012 Total O_3 = 240 ppb Lights on at 1100-1120	No particle formation Small particle generation; increase to 2700/cc in 45 minutes CN continued to increase to 16,000/cc
1142-1210 DARK 1211-1244 LIGHTS 1245-1330 DARK	DMS photolysis with ~300 ppb O_3	O_3 = 300 ppb 1142 - Add 50 ppb DMS 1211 - Lights on	Always high CN conc.
1330-1550	Effect of propene DMS + O_3 + C_3H_6 DARK & LIGHTS	1330 add 200 ppb C_3H_6 DARK CHAMBER 1417 Lights ON 1507 Lights OFF	O_3 decreased more rapidly when C_3H_6 was added
1555-1710	Effect of adding NO in Dark	T.S. ≈ 50 mv O_3 = 230 ppb NMHC ≈ 150 ppb 1555 add 20 ppb NO DARK	Huge increase in CN in dark chamber SO_2 increase - T.S. decrease O_3 decrease
1712-1717 IC			SO_4 = 2.1 $\mu g/m^3$ MSA = <0.2 $\mu g/m^3$ NO_3 = 0.13 $\mu g/m^3$
1740-1950	Effect of lights on DMS, O_3, C_3H_6, NO system + LIGHTS	T.S. = 32 mv O_3 = 298 ppb NMHC = 150 ppb CN = 48K Lights on @ 1740 Added more NO @ 1824	SO_2 increased to ~3.5 ppb T.S. decreased to ~25 mv
1946-1956 IC			SO_4 = 1.41 $\mu g/m^3$ MSA = 1.1 $\mu g/m^3$ NO_3 = 2.11 $\mu g/m^3$

Table 10
NRL SUMMARY OF DMS PHOTOLYSIS EXPERIMENTS (cont.)

TIME	PURPOSE	CONSTITUENTS IN CHAMBER	RESULTS
29 November 1990			
1142-1430	Add components in proportions (except O_3) Photolysis in DMS + O_3 + C_3H_6 + NMHC System	Filtered overnight NMHC=450 ppb Added ~350 ppb O_3 @ 1130 Added ~50 ppb DMS @ 1139 Added ~330 ppb C_3H_6 @ 1142 Added ~80 ppb C_3H_6 @ 1152 Dark System 1259 Lights ON 1349 Lights OFF	Large number of particles formed in the Dark. No increase in particles when lights were turned on.
1430-1600	Add NO to above system Dark System	CN = 38K/cc SO_2 = 0.5 ppb T.S. = 39 mv O_3 = 280 ppb NMHC ≈ 1000 ppb @ 1430 add ~20 ppb NO DARK	Increase in CN from 38K to 180K/cc SO_2 increase over 2 ppb
1542-1547			SO_4 = 4.68 $\mu g/m^3$ MSA = 0.19 $\mu g/m^3$ NO_3 = <0.1 $\mu g/m^3$
1604-2000	Effect of light	Lights on @ 1604 O_3 = 300 ppb TS = 33.6 mv At: 1636 add 20 ppb NO 1800 add 30 ppb DMS 1840 add 20 ppb NO	Addition of NO causes large CN increase
IC 1921-1926			SO_4 = 1.39 $\mu g/m^3$ MSA = 1.38 $\mu g/m^3$ NO_3 = 4.7 $\mu g/m^3$
1930	20 ppb NH_3 added		
IC 2003-2008			SO_4 = 1.04 $\mu g/m^3$ MSA = 1.64 $\mu g/m^3$ NO_3 = 4.3 $\mu g/m^3$

Section 3

REDUCED VISIBILITY IN HAZE OVER THE ARABIAN SEA

3.1 INTRODUCTION

During 1987–89, Calspan provided forecast rules to the Navy for an expert system of fog forecasting at sea (Rogers, 1989). In late 1988, we were asked by the Contract Officer's Technical Representative (Dr. Paul Tag of NOARL West, then NEPRF) to consider possible rules for forecasting haze. The impetus for this request was a haze condition that had been experienced by the CVN Vinson in the Gulf of Oman during August 1988. Although our short term response under the fog forecasting contract was to produce some general rules about haze visibility over the oceans, our long-term goal was the acquisition of aerosol data in this haze off the Arabian Peninsula.

In early 1989, it was decided that Calspan would design and install aerosol acquisition equipment on the CVN Vinson with which the meteorological staff could acquire aerosol samples on a subsequent trip to the region. Because of the CVN Vinson's schedule, it was not until early December 1989 that we were able to visit the Vinson in port, and to finalize design and location of the aerosol acquisition system which was then installed in January 1990. At this time personnel on the Vinson were instructed in the system's operation and in the data handling procedures to be employed.

3.1.1 Equipment

The measurement apparatus consisted of millipore filters through which air was drawn at approximately 10 liters/min via a Gilian AIRCON 520 AC constant flow air sampling system. The filters were exposed on the starboard side of the Vinson's island at the highest manned level. Tygon tubing connected the pump flow to the filters.

Two filters of different pore sizes, 2.0 and 0.4 μm diameter, were used. The standard filter configuration used only the 0.4 μm size. However, to obtain som nformation about the size distribution of the aerosol, a small number of double filter configurations were constructed in which the 2.0 μm filter was placed in series upstream of the 0.4 μm filter. For transport, filter samples were stored in resealable plastic bags both before and after exposure.

The experiment log kept by the Vinson personnel recorded the on and off times of the filter (as well as the filter exposure time from the pump timer, which served to check the filter times), the on and off flow rates and the ship's position at these times. Upon return to port in August 1990, the exposed filters

the log book, copies of the ship's surface observations (NDC Form 3141/2) for the experimental period and the sampling equipment were retrieved and returned to Buffalo by Calspan personnel. The filters were then sent out for global elemental analysis by proton induced x-ray emission (PIXE).

3.1.2 Characteristics of the Data Set

Figure 10 shows the geographical location of the aerosol measurements. Approximately 75% of the observations were taken in the double cross hatched area near 20°N and 60°E off shore of Masirah Island. Another 10% were taken in the northern single hatched area, with the remaining 15% in the southern single hatched area. Most of the observations were taken within 60 nmi of the coast.

Figure 11 shows the time distribution, both by day of the month and time period during the day, for the 32 samples taken within the area outlined in Figure 10. The samples labeled with a 'D' after the number represent the double filter samples. The heavy vertical lines separate the exposure times for the two filters exposed during a single, 24-hour interval (6 AM to 6 AM).

The sampling period naturally divides itself into three portions. The first one extends from 5 May through 18 May during which the ten available double filters were each exposed on the order of eight to ten hours (from sunrise (6 AM local time) to generally mid-afternoon) and the single filters were exposed the remaining portion of the 24-hour day. This period contains the 10% of the observations taken in the northern excursion and approximately half of the central region's observations. The second portion covers 19-23 May when the southern excursion took place, and when only a single 0.4 μm filter was exposed for most or all of each 24-hour day. The third portion covers the remaining observations taken in the central portion of the area, during which the sampling protocol was returned to eight to ten hour filter exposures, starting at sunrise, followed by an observation period to fill out the 24 hours. However, in this case, all observations were taken with a single 0.4 μm filter.

3.1.3 Meteorology of Data Acquisition Period

The meteorology of the observation period was characterized by transition from a winter regime to the summer monsoon. During the first two weeks the region experienced very weak to moderate pressure gradients, with a three-day period of sea breeze circulations. Correspondingly, wind speeds were distributed on either side of the 10-knot value. The next ten days experienced moderate pressure gradients with wind speeds predominantly in the 10-20 knot range. The final five days saw the onset of the summer monsoon with speeds generally between 20 and 30 knots.

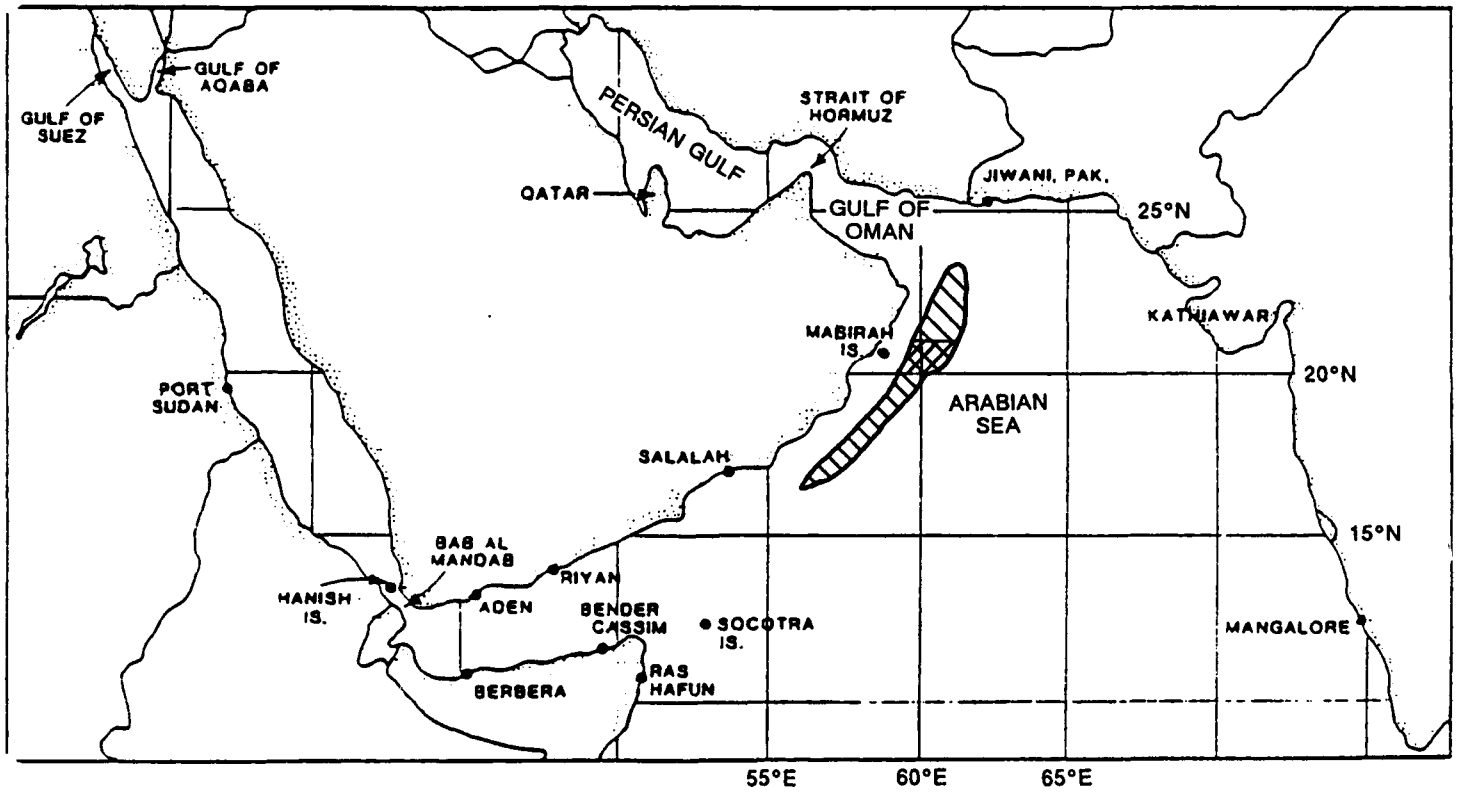

Figure 10 LOCATION OF AEROSOL SAMPLES (HATCHED AREA), MAY 1990

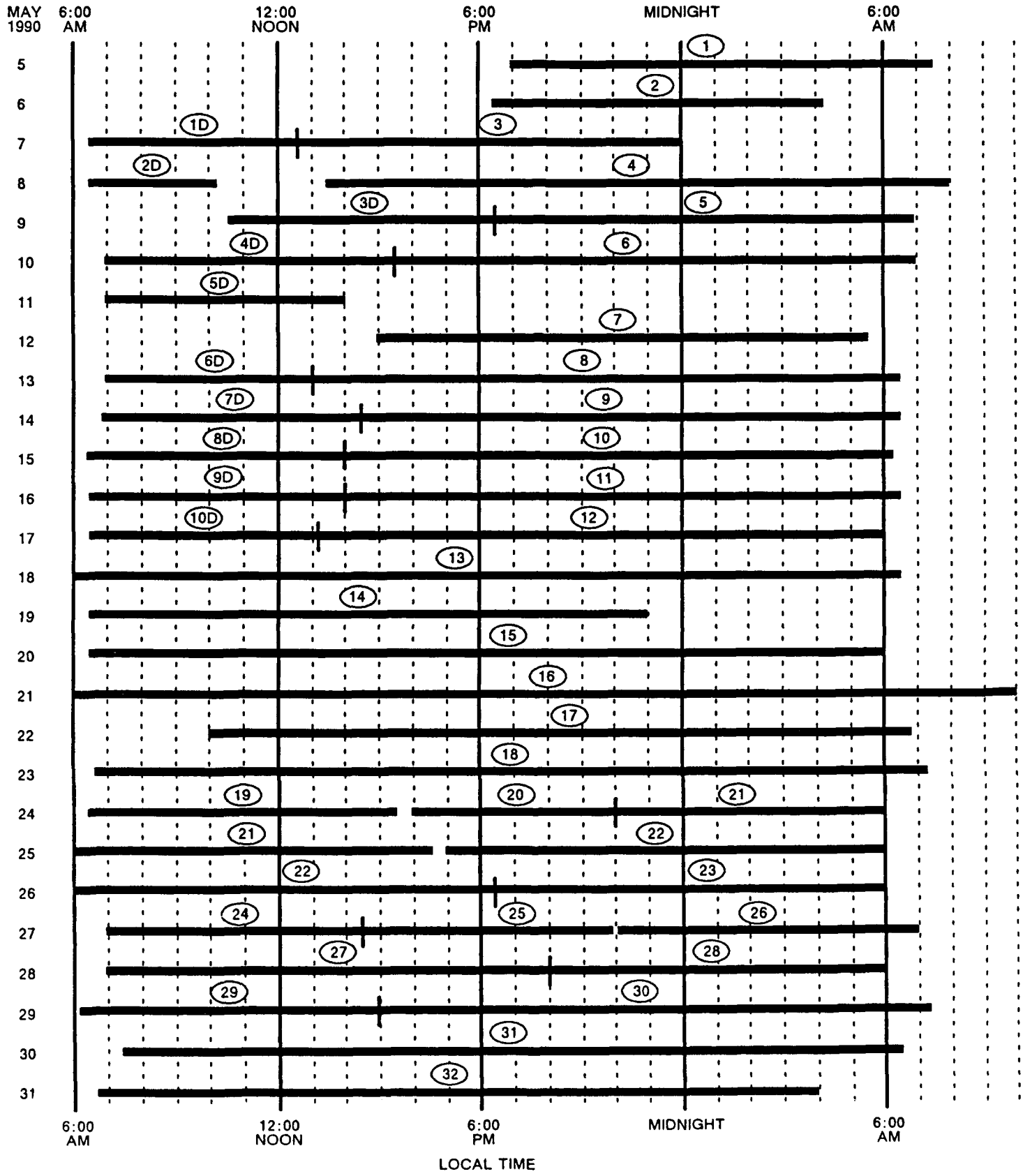

Figure 11 TIME SERIES OF AEROSOL FILTER SAMPLES TAKEN OVER THE ARABIAN SEA NEAR 20°N, 60°E DURING MAY 1990

The days with moderate to strong wind speeds also had wind directions covering the 60° sector from 190° to 250°. The sea breeze days were characterized by wind directions generally spanning the southwest quadrant from 180° to 270°, with a few early morning land breezes blowing offshore from the northwest.

Compared to the August 1988 period when the visibility seldom went above 4–5 nmi for almost two weeks, the visibility during May 1990 was frequently in the 7–10 nmi range.

The major low visibility period occurred from the 13th through the 16th. During this period, not only did minimum visibilities of 4 to 5 nmi occur during the nighttime hours, but maximum visibilities during the day rose only to 7 nmi. Basically, the lowest visibility occurred near sunrise as the relative humidity reached its maximum value and the offshore land breeze peaked at the Vinson's offshore position. The 7 nmi visibilities then occurred during daylight hours as the ship experienced the aged aerosol present in the return onshore flow of the sea breeze circulation.

Toward the end of the month, a constant visibility of 6 nmi throughout the entire day set in as the very strong southwesterly monsoon of summer became established.

3.1.4 Elemental Chemistry of Aerosol Samples

All filter samples were sent out for elemental analysis via proton induced x–ray emission (PIXE). The PIXE analysis provides only global data (i.e., total filter) for elements with atomic weight greater than or equal to that of sodium. Table 11 shows the percentages by mass for the ten most common elements found in these aerosols. The 'D' in the filter run number indicates a double filter configuration. The data included in the table are for the top filter with the 2.0 μm diameter pore size which analysis showed matched the variety of elements found on the single filters. The run numbers in this list account for 42 of the sixty filters supplied for the data acquisition (fifty 2.0 μm pore diameter and ten 0.4 μm pore diameter). Data for the 18 remaining filters are not shown since they were exposed as the Vinson crossed the intertropical convergence zone with its associated convective precipitation.

The elements are arranged left to right in the table as follows: the most abundant continental source elements in this data set, calcium and silicon; next, the sea water based elements, chlorine, sodium, magnesium, potassium and sulfur; then, iron and aluminum, less abundant continental based elements; and finally, titanium, perhaps related to the ship's presence.

The maximum and minimum visibility observed during the filter's exposure period is presented in columns 2 and 3. The period covered by Filters 1 through 6 shows the characteristic diurnal cycle discussed above. Since the double filters (1D, 2D, 3D and 4D) were acquired during the daytime, they only experienced the 10 nmi visibilities. On the other hand, the single filters that were acquired during both the

Table 11
ELEMENTAL MASS CONCENTRATION IN PERCENT FOR AEROSOL FILTER SAMPLES OBTAINED OVER THE COASTAL ARABIAN SEA – MAY 1990

	Visibility (nmi)		Elemental Mass Concentration (%)									
Run	Max	Min	Ca	Si	Cl	Na	Mg	K	S	Fe	Al	Ti
1	7	7	7	30	16	7	4	4	11	10	9	1
2	7	7	5	18	31	18	4	3	9	4	5	1
1D	10	10	6	20	30	17	4	2	8	6	6	1
3	10	7	7	13	5	-	3	1	1	16	4	10
2D	10	10	8	29	22	12	4	2	8	6	6	1
4	10	7	6	19	26	8	3	6	7	14	5	1
3D	10	10	12	26	19	11	4	2	6	12	6	1
5	10	7	11	20	28	14	4	2	7	5	6	1
4D	10	10	11	25	25	10	4	3	8	6	7	1
6	10	7	10	20	34	8	5	2	7	5	7	1
5D	7	5	15	26	25	6	4	2	6	6	7	-
7	10	7	12	21	28	12	4	2	7	6	7	1
6D	7	5	12	22	26	13	4	2	6	6	7	1
8	10	6	11	20	28	14	5	2	6	6	7	1
7D	8	4	16	25	17	7	3	2	6	8	8	4
9	7	5	19	26	16	6	5	3	8	8	9	1
8D	7	5	41	17	10	5	6	1	7	5	4	-
10	10	6	34	21	11	5	6	2	8	6	6	1
9D	7	5	37	22	9	4	6	2	8	6	5	-
11	7	7	22	26	12	7	6	2	8	7	8	1
10D	10	10	18	24	15	6	4	6	8	6	7	6
12	10	5	20	25	15	7	4	2	7	5	12	1
13	10	5	19	27	13	6	4	3	8	9	9	1
14	10	7	15	30	13	8	5	3	6	8	10	1
15	10	7	14	30	15	8	5	3	5	8	10	1
16	10	7	14	34	10	5	5	4	6	10	12	1
17	10	7	16	30	10	4	6	4	8	9	10	1
18	10	7	15	29	13	6	6	3	8	9	10	1
19	10	7	11	22	25	14	4	3	7	6	7	1
20	10	7	9	21	25	16	4	2	9	5	7	1
21	10	4	9	16	35	17	4	2	7	4	5	1
22	10	7	8	11	37	17	4	3	6	11	4	1
23	10	7	10	14	42	10	5	2	6	3	6	1
24	10	10	6	10	48	18	4	2	7	2	2	1
25	10	7	5	11	45	21	4	2	6	2	3	-
26	10	7	4	7	50	23	4	1	5	2	2	-
27	10	7	7	10	49	15	5	2	7	2	3	-
28	10	7	5	6	56	18	3	3	5	1	2	-
29	6	4	6	9	47	22	4	2	6	2	3	-
30	7	6	8	10	49	10	5	2	7	3	4	-
31	7	6	3	4	56	22	4	2	5	1	1	-
32	7	7	3	4	56	25	4	1	5	1	1	-

day and night, show both the visibility values experienced during the diurnal cycle. Filters 1 and 2 were both run entirely at night and therefore show only 7 nmi visibilities. Filters 1 to 2D were taken on the northwest track as the ship approached 20°N and 60°E while Filters 4 through 6 were taken during the excursion to the northern portion of the sample area as shown in Figure 10.

After a transition period (Filters 5D to 7D) during which the ship neared the coast to anchor off Masirah Island, the most consistent period of reduced visibility was encountered during exposure of Filters 9 through 13, when the ship remained within 60 nmi of the coast.

During Filters 14 through 28, the characteristic diurnal visibility cycle was dominant, as the ship first performed the southwestern excursion (Filters 14 to 18) and then returned for the second major sampling of the area centered on 20°N, 60°E. After that, the ship exited the Arabian Sea on a southeasterly course.

The most obvious feature of this table is that the period of most consistent lowest visibility, Filters 9 to 13, corresponds to the period of highest percentages of Ca along with the lowest percentages of Cl. These features suggest that the lowest visibilities occurred with air of continental origin.

The above conclusion is confirmed by Table 12, in which the wind direction distribution during each filter exposure is shown for Filters 8 through 13. As seen in Figure 11, this sequence of filters is continuous in time, so that Table 12 presents a complete distribution of wind direction during this six-day period.

Notice that three of the five filters with the highest Ca content, Numbers 9, 8D and 9D, experienced winds with directions greater than 260°, and these wind directions were also the directions from the ship to the nearest land. Of these three filter samples, the one nearest to the shore, and also the one with the largest percentage of offshore flow (50%), was 8D, which turned out to have the largest percentage of Ca. Although the 300° wind direction occurred at the same distance from shore for both Filters 9 and 8D, it contributed to only about 6% of the total exposure time for Filter 9, with the corresponding Ca percentage being much less, about half of that found on Filter 8D.

Of greater interest in terms of reduced visibility in haze associated with continental air, is Filter 10, which showed the third highest Ca percentage, but experienced only slightly more than 10% offshore flow. The other 90% of the flow was primarily from 150° to 170°, which turned out to be predominantly the continental air of the early morning land breeze returning landward in the afternoon sea breeze. Therefore, although this third-highest Ca percentage value had little offshore flow, the sampled air was still primarily continental, although the aerosol had aged during its presence over the ocean

Table 12
NUMBER OF OCCURRENCES OF HOURLY WIND DIRECTION DURING EXPOSURE OF SELECTED AEROSOL FILTERS FROM USS VINSON, MAY 1990

Filter	Starting Time (GMT) and Date	Wind Direction (10's of Degrees) 14 15 16 17 18 19 20 21 22 23 24 25 26 27 28 29 30 31	Calcium Weight Percent
8	1242/13	6 7 2 4 1	11
7D	0247/14	2 3 1 3	16
9	1025/14	3 2 1 1 1 2 1 2 1 1 1	19
8D	0231/15	1 3 1 2 1 3	41
10	1000/15	1 5 3 5 1 3 3 1 1 2	34
9D	0230/16	1 1 1 2 1 2 1	37
11	1026/16	1 2 2 9 2 3 2	22
10D	0235/17	1 2 3 1 2	18
12	0913/17	1 8 5 12	20
13	0200/18	1 3 2 14 5 1	19
13 Off	0200/19		

As pointed out in connection with Figure 11, the double filters were exposed from around 0600 to 1400 local time, with the single filters exposed over the remaining 16 hours. Thus, the double filters were exposed in both the offshore portion of the sea breeze and the onset of the onshore breeze. Conversely, the single filters were exposed both during the onshore sea breeze and the beginning of the offshore land breeze. These features can be seen in Table 12 for the single Filters 9–11 with the wind direction extending into the south–southeast and the broad span of wind directions centered around 180°. For the double Filters (8D, 9D, and 10D) the wind direction distribution is narrower and centered near 270°.

From these data, one can see that the sea breeze regime lasted three days, starting on the 14th (Filter 9) and extending through the morning of the 17th (Filter 10D). This is also the period during which the Ca percentage values were the highest and the Cl percentage values were the lowest, i.e., the air was of continental origin and the visibility was consistently low in the accompanying haze.

Subsequent Navy sponsoring by the then NOARL Atmospheric Directorate, Dr. Paul Tag, COTR (now NRL Monterey), has funded an ongoing effort to develop a technique to forecast the lowered visibility in this haze, based in part on these previously acquired aerosol samples.

Under this companion contract, analyses which were performed on the filter samples were: 1) size distribution and concentration via scanning electronic microscopy (SEM) and elemental composition of particles via energy dispersive x-ray analysis (EDXA), 2) hygroscopicity tests to examine deliquescence points of the aerosol and 3) ion chromatography to identify ions, e.g., $SO_4^=$ and NO_3^-. The results of these analyses are to be published in Rogers (1992).

Section 4

SOME CAUSES FOR THE VARIATION OF DIMETHYLSULFIDE EMISSION RATES FROM WATER SURFACES*

4.1 INTRODUCTION

As part of world-wide sulfur budget studies during the past two decades, numerous authors have attempted to estimate the total emission of dimethylsulfide (DMS) from ocean and continental surfaces (Lovelock et al., 1972; Cline and Bates, 1983; Barnard et al., 1982; Andreae and Raemdonck, 1983).** Others have examined chemical processes in the atmosphere that lead to production of hygroscopic aerosol from DMS (Saltzman et al., 1983 and 1985; Hatakeyama et al., 1985; Cox and Sandalls, 1974), and growth of that aerosol to cloud nuclei (Hoppel et al., 1987, Kreidenweis and Senfeld, 1988) and the return of the sulfur to the surface by precipitation (Andreae et al., 1988). The purpose of this study was to attempt to relate local emission rates of DMS from the sea surface to the production of local marine boundary layer aerosol. That part of the study that required developing an understanding of processes that control DMS emission rates is reported here.

Experimental efforts on this program were performed in conjunction with the Office of Naval Research (ONR) Marine Microlayer field exercises at the IC Darling Center in Maine (May and September, 1987), the Bermuda Biological Station (May, 1988) and Scripps Institute, La Jolla, California (September, 1988). This association was particularly valuable in that it permitted us to examine DMS emission rates with the added data base characterizing the uppermost layer of the ocean. Microlayer and bulk ocean water samples were acquired from a small boat operated in the Damariscotta River estuary in Maine, on the RV Weatherbird off Bermuda and the RV Robert G. Sproul between La Jolla and San Clemente, California

It is generally agreed that the gas transfer rate from ocean to air is limited by the molecular diffusion of gas through a surface layer of the order of 50 microns thick at the water surface (Broecker and Peng, 1974; Liss and Slater, 1974). Measurements of DMS emission rates were made from surfaces of fresh bulk sea water under a variety of controlled and well-characterized conditions Aliquots of bulk and microlayer water samples were sparged with dry nitrogen to determine DMS concentration before emission measurements were made, thereby providing data on the distribution of DMS in surface waters.

---

* Submitted to Journal of Physical Oceanography Authors: Roland J. Pilie', Bruce J. Wattle and John G. Michalovic

** References for this section are self contained in Section 4.6.

Emission rates were measured on separate aliquots of these same water samples. Data were acquired from quiescent and mixed conditions in some cases, from unskimmed surfaces in others, and from surfaces from which the microlayer had been skimmed and then replaced in still other cases. Through these experiments, we attempted to define the parameters that are important to and develop a consistent picture of the emission processes that take place.

4.2 EXPERIMENTAL AND ANALYTICAL PROCEDURES

The gold sorption technique described by Braman et al. (1978) was used for all DMS analyses. In our system, the DMS was sorbed on gold-coated pyrex beads (60 to 80 mesh), then desorbed at 485C into a nitrogen stream, passed through a moisture trap at 0C and into a cryogenic trap at liquid nitrogen temperature. The cryogenic trap was then heated in preparation for injection of the sample into a Varian Model 6000 gas chromatograph (GC) controlled by a model 401 Data System. Quality control tests demonstrated that the sorption-desorption-injection train had an overall recovery factor of approximately 98% for DMS.

The basic experimental approach used for emission rate determination was to place one liter of fresh, bulk ocean water in a 170 mm diameter silanized crystallizing dish housed in a closed 8-liter Teflon-lined container that was continuously flushed with dry nitrogen at a rate of one liter per minute through a moisture trap into a gold bead sorption tube. Flow rates into the head space of the container and into the sorption tube were measured continuously to account for leaks, should they occur. In a typical experiment, the head space was flushed for 10 minutes to establish a steady state emission rate before attaching the sorption tube for either 30 or 60 minutes of DMS collection. From geometric considerations, it was apparent that 19% or 10%, respectively, of emitted DMS remained in the head space at the end of these collection times. However, quality control measurements of DMS recovered after direct injection into the head space ranged from 41 to 60% and averaged near 50%, indicating substantial losses to the container walls. A factor of two was used to correct for the recovery deficit in all emission data presented below. Variability in recovery rate is by far the greatest source of overall error in the measurement of emission rate, which is estimated to be $\pm$ 20%.

Measurements of DMS concentration in sea water were made using the sparging technique described by Andreae and Barnard (1983) modified for collection of DMS with the gold bead sorption tubes. During the Bermuda and San Diego field programs, aliquots of the same water sample used for emission measurements were sparged for DMS concentration determination.

The gold bead sorption tube-GC measurement apparatus was calibrated daily by injecting known quantities of DMS into a nitrogen stream entering the sorption tube and proceeding with the analytical sequence. Spikes and blanks were injected in the same way occasionally throughout each day. Daily calibration curves for the Maine and Bermuda field trips show that the response of the system is repeatable, with a standard deviation between 1.58 and 1.75 ng DMS for mass levels about 110 ng. Based on these numbers, the errors for measurement of DMS concentration in water are less than 5% for all concentrations greater than 300 ngl^{-1} and approximately 10% for concentrations of less than 300 ngl^{-1}. The repeatability of the measurement system during the San Diego experiments was somewhat worse, with standard deviation of 2.7 ng at levels below 40 ng and $\pm$ 6 ng above 40 ng. Measurement errors are less than $\pm$ 15% for all water concentrations in excess of 200 ngl^{-1}. All DMS concentrations encountered in San Diego offshore waters were greater than 200 ngl^{-1}.

Bulk water samples were collected in crystallizing dishes from the Damariscota Estuary in Maine and from Ferry Reach in Bermuda, and analysis initiated within 30 minutes. Ocean water samples were collected from 500 to 1000 m offshore in silanized two liter bottles in Bermuda, and analysis initiated within about one hour. Most of the water samples collected in San Diego nearshore waters were sparged immediately. In some cases, samples were stored in 150 ml serum bottles at 35°F for analysis with shorebased equipment. Quality control samples of this kind showed that retention beyond approximately six hours resulted in significant increases in DMS concentration that were not acceptable. Unless otherwise stated, data presented in this paper were analyzed within six hours of collection. All San Diego samples used for DMS emission measurements were collected, either at the end of the Scripps pier or from the RV Sproul within 1000 meters from shore, and analysis was initiated within an hour.

4.3 DMS EMISSION RATE CHARACTERISTICS

Data from the three field programs were analyzed to gain knowledge about: 1) the influence of mixing on the DMS emission rate, 2) diurnal variations in DMS concentration, 3) the effect of DMS concentration in the bulk sea water on the emission rate, 4) the DMS concentration in samples of microlayer water and bulk sea water collected simultaneously, and 5) the influence of the microlayer in controlling DMS emission rate. The resulting emission rate data are compared to calculations based on Fick's law, using constants derived from the literature.

4.3.1 The Influence of Mixing

The thickness of the surface through which molecular diffusion of DMS occurs varies with the degree of mixing which, in the ocean, is attributable to wind-driven wave actions. To demonstrate the importance

of this parameter, we measured the emission rate from samples of estuary water (Damariscotta, Maine) in the quiescent state and with the minimum achievable mixing using a magnetic stirrer. First, we established that the reduction of DMS concentration in a one liter sample due to emission during one experiment did not significantly affect emission in an immediate rerun with the same sample. This permitted experiments to be performed with the same water sample, first quiescent and then mixed. The results are presented in Figure 12. Stirring produced an increase in mean emission rate above the quiescent state from an average of 1.86 to 4.8 $\mu g\ m^{-2}\ hr^{-1}$, a factor of 2.6. The minimum increase was a factor of 1.9 and the maximum was 3.1.

4.3.2 Diurnal Variations

Diurnal variations in DMS emission rate have been hypothesized. Some verifying data exist for coastal waters, but few at sea. Our experience confirms these prior observations. Jorgensen and Okholm-Hansen (1985) observed diurnal variations in a Danish Estuary. We obtained two independent data sets in the Damariscotta (Maine) Estuary which also demonstrate this effect. The first data set, presented in Figure 11, relates DMS emission rate variations to cloud cover. The second data set, presented in Figure 13, relates the atmospheric concentration of DMS within one meter above the water surface to integrated incident sunlight at the surface since sunrise. Data obtained between seven and 10 meters above the water, where DMS concentration was typically a factor of about five smaller (mean equal to 13 vs 58 ngm^{-3}), do not show a relationship to integrated solar intensity. The ability to observe a diurnal effect was undoubtedly due to the short fetch over the estuary, which insured that DMS emitted from the estuary did not have sufficient time to mix more than a few meters into the atmosphere.

4.3.3 The Influence of DMS Concentration in Sea Water

Initial attempts to relate emission rate, E, to DMS concentration, C, in sea water were made in Bermuda. All but one of the samples were drawn from Ferry Reach, a 2 km long, 200 m wide pass connecting St. Georges Harbor on the east to Castle Harbor and the Atlantic on the north. Similar experiments were also conducted during the San Diego cruise. Water samples for this data set were collected from the Scripps Pier. All water samples were drawn from within 10 to 20 cm of the surface. The sea water DMS concentration versus emission rate results are presented in Figure 14.

Linear regressions of the two data sets yield

$$E = 3.7 \cdot C \qquad (1)$$

with a correlation coefficient (R) of 0.88 for Bermuda and

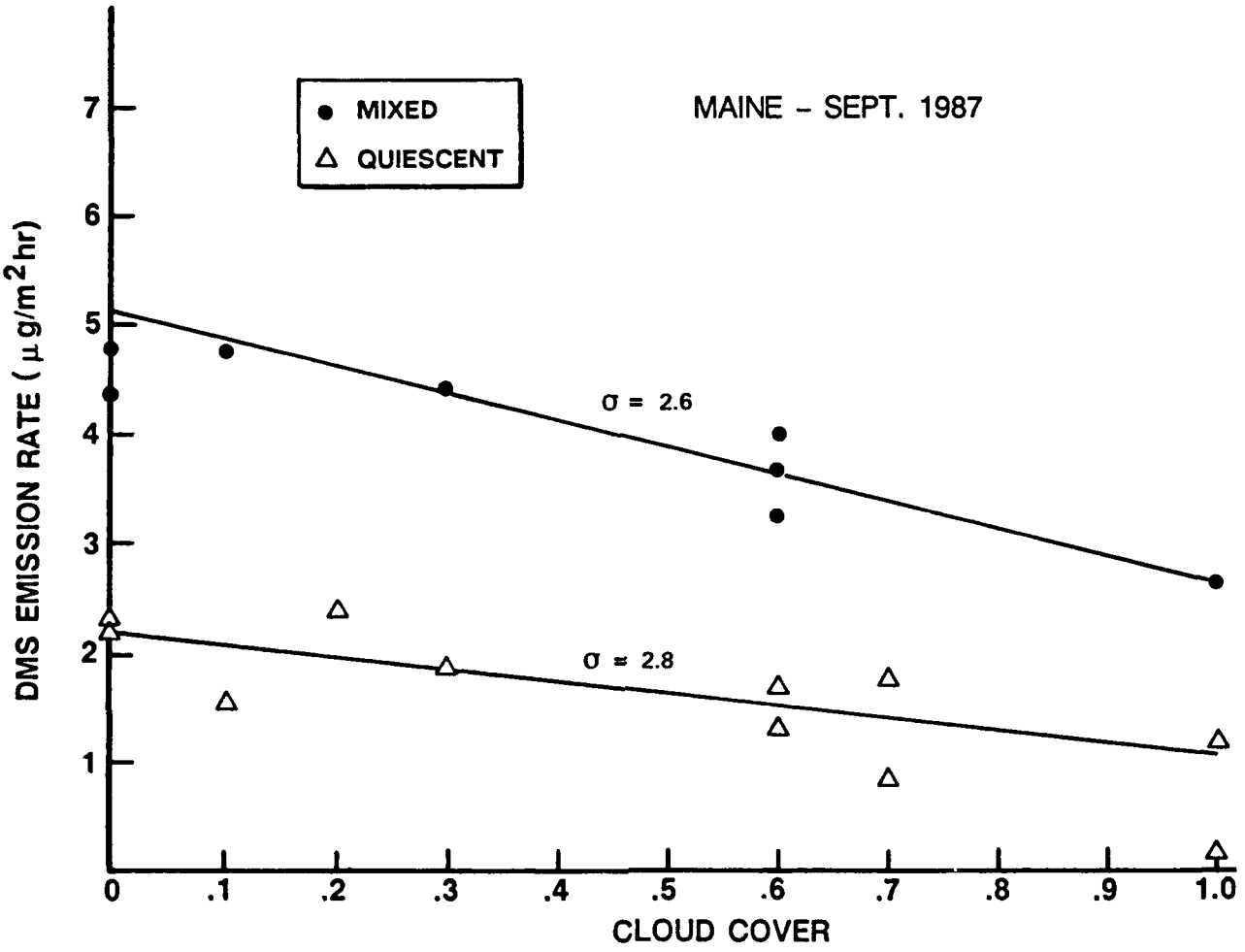

Figure 12 THE INFLUENCE OF MIXING AND CLOUD COVER ON DMS EMISSION RATE

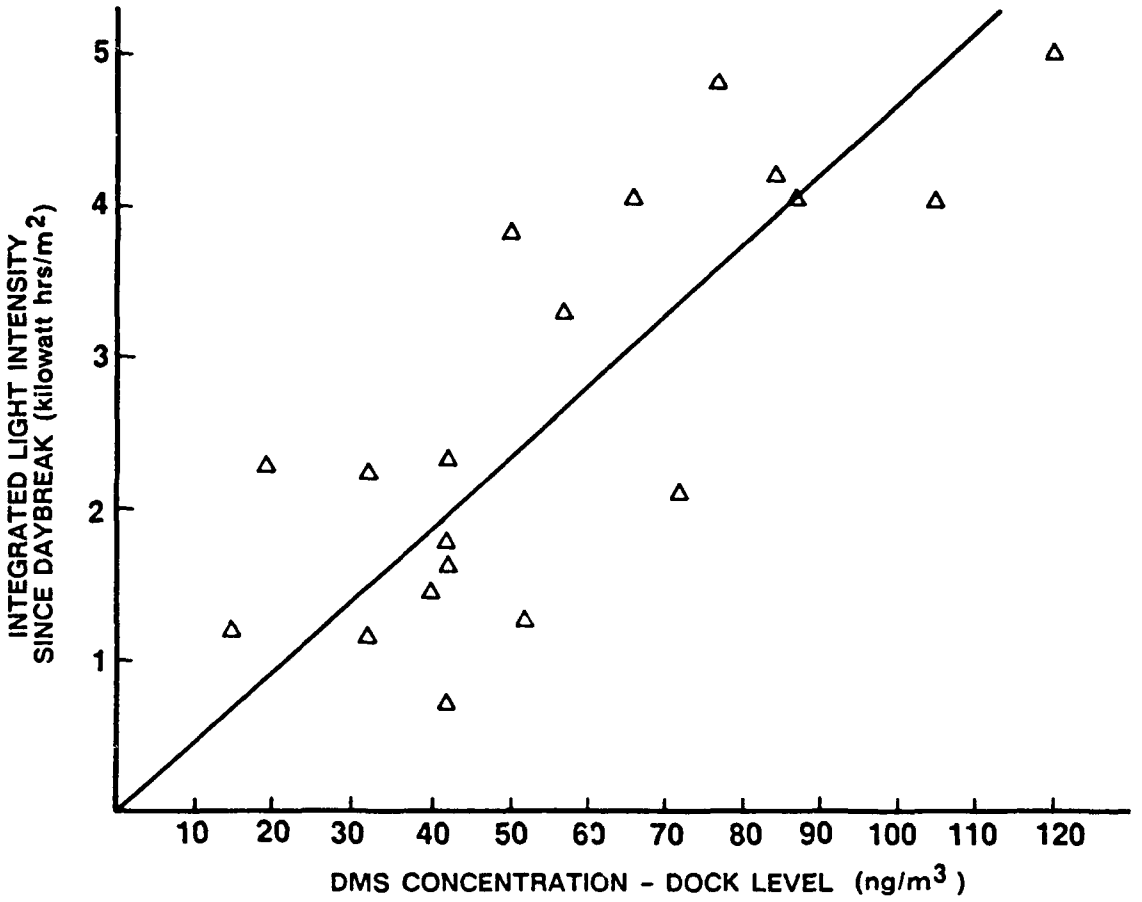

Figure 13 DMS CONCENTRATION AS A FUNCTION OF INCIDENT LIGHT

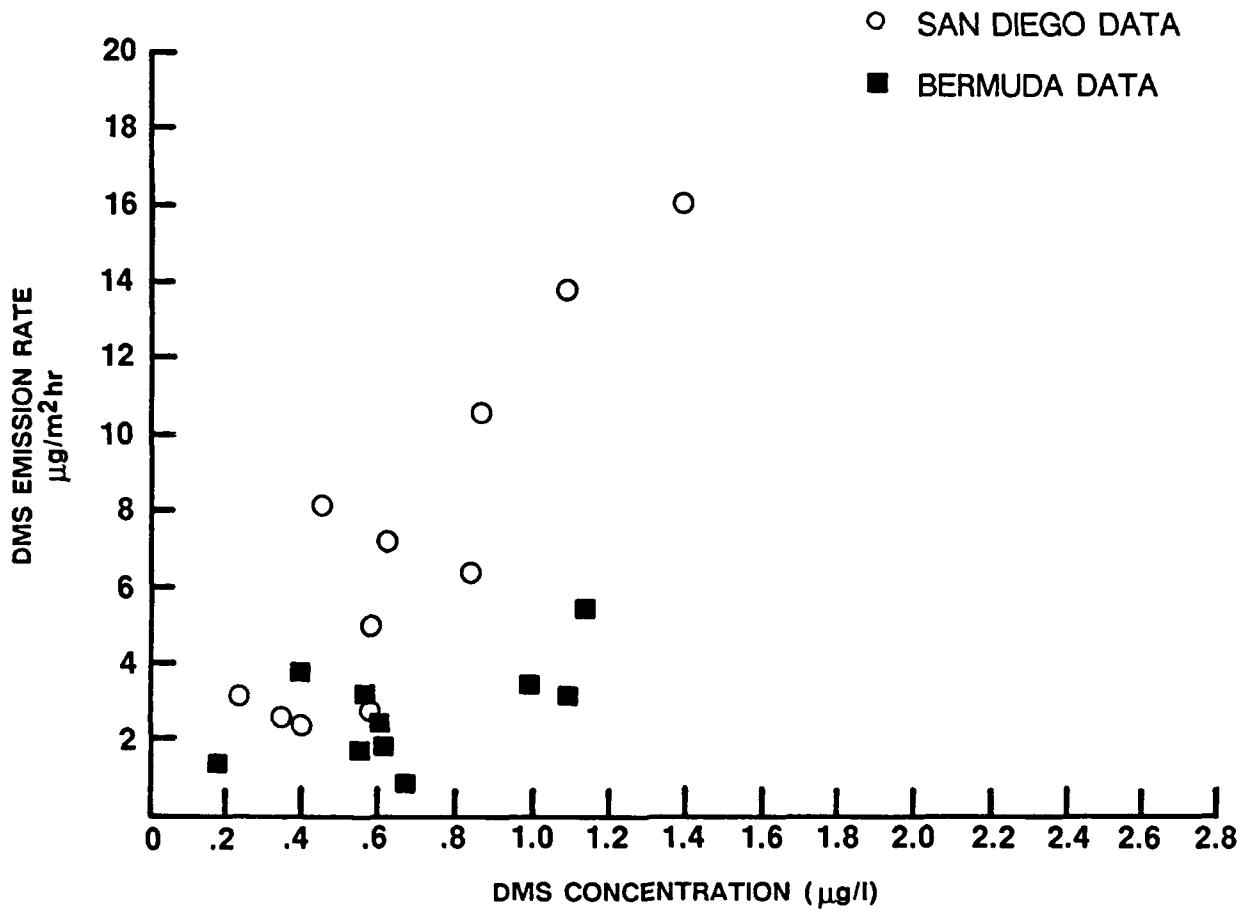

Figure 14 DMS EMISSION RATE AS A FUNCTION OF DMS CONCENTRATION IN SEA WATER

$$E = 11 \cdot C \qquad (2)$$

with $R = 0.95$ for San Diego; E is in $\mu g\ m^{-2}\ hr^{-1}$ and C is in μgl^{-1}. All measurements used to derive the above constants were obtained with quiescent water. The Maine data showed that moderate mixing increased emission rate by an average factor of 2.6, suggesting that the above constants should be increased to 9.6 and 28.6, respectively, when comparing experimental and theoretical results representative of ocean surfaces.

The Bermuda data shown in Figure 14 represent two apparently different regimes within Ferry Reach, neither of which is representative of ocean water. Between 1000 LDT time on 14 May and 2040 LDT on 19 May, the mean concentration of DMS in Ferry Reach was 0.5 $\mu g\ \ell^{-1}$ ($\sigma = 0.057$). From 2040 LDT on 19 May through 20 May, the mean concentration increased to 0.87 $\mu g\ \ell^{-1}$ ($\sigma = 0.26$). During the latter time period, four concentration measurements made from sea water collected in the open ocean (~ 5 km from Bermuda) averaged 0.18 $\mu g\ \ell^{-1}$ ($\sigma = 0.003$).

Similar variability is evident in data obtained near shore off La Jolla in September, 1988, as shown in Table 13. In this case, the change may have been due to a small change in location rather than a change in water characteristics at one location. Because of strong southerly winds on 20 September, the Sproul moved from the vicinity of the Scripps Pier to the protected waters of La Jolla Bay, less than 4 km away, but in the vicinity of the highly populated tourist beaches of La Jolla Point. These data all demonstrate that DMS concentration in sea water is highly variable, a conclusion reached by several previous authors.

Table 13
SEA WATER DMS CONCENTRATION OFF LA JOLLA, CA

Dates	Concentration ($\mu g\ell^{-1}$)	σ ($\mu g\ell^{-1}$)
15 September - 19 September	0.50	0.20
20 September	2.20	0.75
21 September - 27 September	0.65	0.25

4.3.4 Microlayer vs Bulk Water DMS Concentrations

On five occasions during the San Diego cruise, samples of microlayer water obtained from Dr. Nelson Frew of Woods Hole were analyzed for DMS concentration within six hours of collection. On three other occasions, analysis was delayed one to three days. Except for one day (21 September), a bulk water sample (at a depth of 10 cm) was obtained at approximately the same time for comparison with the

microlayer sample. One sample of microlayer water collected in open water off Bermuda by Dr. David Carlson, Oregon State University, on 20 May yielded a value of 0.40 $\mu g \ell^{-1}$, a factor of two greater than that of the four bulk ocean water samples on the same day. The results are presented in Table 14.

It is apparent from Table 14 that the most common situation is for the DMS concentration in the microlayer to be two or more times as high as the bulk water with which it is associated.

One question that is immediately asked after review of such data is whether the presence of a visible slick is indicative of high DMS concentrations in the bulk water beneath it. On two different occasions during the San Diego cruise, bulk water samples were collected sequentially from the centers of the slick and slick-free regions during transects of the striated areas. Samples were stored in sealed serum bottles for subsequent DMS concentration analysis. Time constraints prevented analysis for a day after collection in each case, destroying the validity of the absolute values determined. In both cases, the first with six

Table 14
MICROLAYER - BULK WATER PAIRS

Date	Bulk Water DMS Concentration ($\mu g \ell^{-1}$)	Microlayer Water DMS Concentration ($\mu g \ell^{-1}$)
SAN DIEGO DATA		
September 15	0.64	1.39
September 16	0.54	1.30
September 21	No simultaneous sample	0.30
September 22	0.23	1.79 2.06
September 26	0.41* 0.38*	2.01
The above samples were analyzed within six hours. The samples below were analyzed upon return to shore on 26 September		
September 23	1.94*	1.94
September 24	1.09*	2.57
September 25	0.83*	9.7
BERMUDA DATA		
May 20	0.195	0.400

samples and the second with five, the bulk water DMS concentration in the slick and slick-free regions agreed to within 2%. Thus, it was indicated that the presence of a slick has no correlation with the concentration of DMS in the bulk water beneath it.

4.3.5 The Influence of the Microlayer

Initial attempts to determine the relationship of DMS emission rate to characteristics of the microlayer focused on the possible influence of surface tension. Extensive data obtained during the three field programs by measuring surface tension with a conventional tensiometer and Wilhelmiung plate before and after measurement of DMS flux revealed no evidence of correlation. We next considered methods by which we could skim the microlayer from water samples prior to measurement for comparison with similar measurement with unskimmed water, but were not able to obtain reproducible results.

The procedure which resulted in the most definitive data required measurement of emission rate from a sample of sea water, the careful addition of a sample of microlayer water to the surface using a micropipette with its orifice half submerged in the bulk sample and the immediate remeasuring of emission rate. In some cases, the microlayer was stripped from the surface with clean aluminum foil prior to the initial measurement. Microlayer water was provided by Dr. Frew and Dr. Carlson. The results are presented in Table 15.

The conclusion drawn from the data in Table 15 is that the addition of small quantities of microlayer water (1/2 to 1% by volume of bulk water) to the surface significantly increased the emission rate of DMS. Careful examination of the data shows that of the twelve experiments of this type, the emission rate increased ten times, remained unchanged once and decreased once. Increases ranged from 6% to 40% while the decrease was 13%.

4.4 COMPARISON WITH FICK'S LAW

It was shown earlier that Equations (1) and (2) are reasonably representative of emission rate versus bulk water concentration data obtained in Bermuda and San Diego, respectively. Let us now compare rates computed with these expressions, using constants characteristic of moderate mixing, with theoretical rates using the two applications of Fick's Law, according to Broecker and Peng (1974) and Liss and Slater (1974).

A bulk water DMS concentration equal to 0.1 $\mu g \ell^{-1}$ and a value of 5.2×10^{-2} hr cm^{-1} for the resistance to gas exchange from liquid to air (derived from constants given by Liss and Slater, 1974) are used. The mean thickness of the stagnant layer for the world's oceans is assumed to be 30 μm (Broecker

Table 15
THE INFLUENCE OF THE MICROLAYER ON DMS EMISSION

Experiment No.	DMS Concentration ($\mu g \ell^{-1}$) Bulk	Microlayer ****	Water	DMS Emission Rate ($\mu g m^{-2} hr^{-1}$) Skimmed Water	Add Microlayer Water*	% Change ***
San Diego Data						
1	1.4		16	16		
2	.23	2.1	3.2	3.6	3.6	0%
3	.87	4.5	10.6	10.2	14.4	+38%
4				7.0	9.8	+40%
5	.46	9.9	8.2	9.0	12.0	+33%
6	.62	4.0	7.2		10.0	+39%
7	.94	10.1	1.3		1.5	+15%
8**	.88	17.0		13.2	16.4	+20%
Bermuda Data						
1	.62			1.9	2.1	+6%
2	.54			2.4	2.6	+6%
3	1.14			5.5	6.8	+23%
4	.53			2.5	2.8	+10%
5	.40			3.8	3.3	-13%

* In Bermuda experiments, 5 ml of microlayer water was added. In San Diego experiments, 10 ml of microlayer water was added.

** In Experiment No. 8, microlayer water was added for initial measurement and then skimmed for the second measurement.

*** The percent change caused by adding microlayer to previous condition.

**** The data in this column were acquired when microlayer water was placed on the bulk water, which was for some samples several days after sample collection. Hence, the very large concentrations of DMS.

and Peng, 1974). The diffusion coefficient for DMS was assumed to be 1.3×10^{-5} cm^2 sec^{-1} (Cline and Bates, 1983). The results are presented in Table 16.

It is apparent from Table 16 that the San Diego data are in reasonably good agreement with theory while the Bermuda data are low by a factor of 3 or 4. What is most perplexing, however, is that the measured concentrations of DMS in bulk and microlayer water (Table 14) indicate a concentration gradient across the molecular diffusion layer that is opposite to that required for application of Fick's Law. Consideration of how the concentration distribution evolves and implications of that distribution relative to DMS emission is certainly warranted.

Table 16
COMPARISON OF EXPERIMENTAL AND THEORETICAL VALUES FOR EMISSION RATE OF DMS. UNITS ARE ($\mu gm^{-2}hr^{-1}$)

Experimental		Theoretical	
Bermuda	San Diego	B&P 1974	L&S 1974
6.50	27.6	26.3	19.2

We have considered two explanations for the evolution of this distribution: the microlayer could be a more prolific source of DMS than the bulk water, or it could be a strong sink of DMS. Carlson et al. (1988) and Cullen et al. (1989) show that biological activity in the microlayer was significantly greater than in the bulk water in the specific samples that were analyzed for the DMS data presented in this paper. It is reasonable to expect, therefore, that the microlayer is the more prolific source.

Two possibilities exist that could cause the microlayer to be a sink for DMS. If the solubility of DMS in microlayer water were greater than in bulk water, it would, in essence, extract DMS from the bulk. Furthermore, if the diffusivity of DMS within the microlayer were much smaller than in the bulk, it would also serve as a sink. Such a situation could occur if DMS molecules within the microlayer are or become attached to larger, less mobile particles such as fragments of decaying plankton or large protein molecules. These hypotheses are plausible in view of the biological activity mentioned above. In order to make the concentration measurement, however, DMS bonding to the larger bodies would have to be weak enough so that its release would occur in the sparging process.

Consider now the implications of these hypotheses relative to DMS emission rates. If the microlayer is a source of free DMS (i.e., diffusivity equal to that in the bulk) the high measured concentration at the surface would inevitably result in a higher gradient that would cause a larger emission rate than predicted with bulk concentrations. Since this is not the case, either one or both of the processes that would lead to the retention of DMS in the microlayer must occur.

We are most comfortable with a scenario in which the microlayer is a prolific source of DMS, most of which remains bonded to phytoplankton fragments or zooplankton waste products and thus does not participate extensively in emission. The prime source of DMS for emission remains free DMS from the bulk water. The fraction of microlayer-produced DMS that becomes dissociated from decaying phytoplankton is responsible for the observed increase in emission rate when microlayer water is replaced on the sample surface. The enhanced concentration of the fertile bulk waters of Ferry Reach over nearby

ocean water may also be due to DMS associated with plankton fragments, and, therefore, not fully available for emission, which fits with the reduced emission rates in the Bermuda data.

4.5 SUMMARY AND CONCLUSIONS

The emission rate of DMS and factors controlling the emission rate were investigated during four field experimental efforts. Sorption tubes containing gold-coated beads were used to collect DMS, followed by analysis with a gas chromatograph. This analytical technique was calibrated daily and a typical measurement error of $< \pm 10\%$ was determined for bulk water DMS concentration measurements and $\pm 20\%$ for DMS emission rate measurements.

Agitation of bulk ocean water samples resulted in an increase in the DMS emission rate by a factor of 2.6 above the emission rate for a quiescent sample. The agitation reduces the thickness of the molecular diffusion layer at the water surface, and may also act to release DMS otherwise bound to organisms in the water sample.

The observed low-level increase in atmospheric DMS concentration with integrated light intensity after daybreak is consistent with anticipated diurnal variations in emission rate. Evidence is presented that indicates the extent of diurnal variation is negatively correlated with cloud cover.

Data are presented showing that DMS concentration in the marine microlayer is usually a factor of two or more greater than that in the bulk water 10 to 20 cm beneath. Experiments in which microlayer water was added to the surface of bulk water suggest that the presence of a well-developed microlayer can cause the DMS emission rate to be 10% to 40% larger than when no microlayer exists (other conditions being the same). This appears to be a subdued response to the increase in surface DMS concentration in the surface layer relative to the bulk water.

In agreement with Fick's law, DMS emission rates are directly proportional to DMS concentration in the bulk water, with the proportionality constant differing by a factor of three for the different sites studied. However, a dichotomy exists in that the concentration gradient immediately beneath the surface (i.e., through the microlayer) is opposite in direction to that on which Fick's Law is based. To relieve this dichotomy, we have hypothesized that the excess DMS in the microlayer water is trapped on decaying phytoplankton and therefore participates only to a small extent in emission to the atmosphere. The trapping hypothesis also fits the observed subdued response of emission rates to high DMS concentration in the microlayer, and may explain the factor of three difference in the proportionality constant relating emission rate to bulk water concentration at the two experimental sites.

4.6 REFERENCES

Andreae, M.O. and Hans Raemdonck, "Dimethylsulfide in the Surface Ocean and the Marine Atmosphere: A Global View," Vol. 221, *Science*, 19 August 1983, pp. 744–747.

Andreae, M.O., Berresheim, H., Andreae, T.W., Kritz, M.A., Bates, T.S., and Merrill, J.T., "Vertical Distribution of Dimethylsulfide, Sulfur Dioxide, Aerosol Ions, and Radon over the Northeast Pacific Ocean," *J. of Atmosphere Chem.*, 6, (1988), pp. 149–173.

Barnard, W.R., Andreae, M.O. and Watkins, W.E., "The Flux of Dimethylsulfide from the Oceans to the Atmosphere," *JGR*, Vol. 87, No. C11, pp. 8787–8793, October 20, 1982.

Braman, R.S., Ammons, J.M., and Bricker, J.L., "Preconcentration and Determination of Hydrogen Sulfide in Air by Flame Photometric Detection," *Anal. Chem.*, Vol. 50, No. 7, June 1978.

Broecker, W.S. and Peng, T.H., "Gas Exchange Rates Between Air and Sea," Tellus XXVI (1974), 1–2.

Carlson, Kantz and Cullen. Description and Results of a New Surface Layer Sampling Device/Deep Sea Research, Vol. 35, Page 1205, 1988.

Cline, J.D. and Bates, T.S., "Dimethylsulfide in the Equatorial Pacific Ocean: A Natural Source of Sulfur to the Atmosphere," *Geophys. Res. Ltr.*, Vol. 10, No. 10, October 1983.

Cox, R.A. and Sandalls, F.J., "The Photo-Oxidation of Hydrogen Sulfide and Dimethylsulfide in Air," *Atmos. Env.*, Vol. 18, pp. 1269–1281, 1974.

Cullen, McIntire and Carlson (1989). "Distribution and Activity of Photoautotropes in Sea Surface Films," Marine Progress series. In Press.

Hatakeyama, S., Izumi, K., and Akimoto, H., "Yield of SO_2 and Formation of Aerosol in the Photo-Oxidation of DMS Under Atmospheric Conditions," *Atmos. Env.*, Vol. 19, No. 1, 1985, pp. 135–141.

Hoppel, W.A., Fitzgerald, J.W., Frick, G.M., Larson, R.E., and Wattle, B.J., "Preliminary Investigation of the Role that DMS and Cloud Cycles Play in the Formation of the Aerosol Size Distribution," NRL Report 9032, July 1987.

Jorgensen, B.B. and Okholm-Hansen, B., "Emissions of Biogenic Sulfur Gases from a Danish Estuary," Vol. 19, No. 11, *Atmospheric Environment*, pp. 1737–1749, 1985.

Kreidenweis, S.M. and Seinfeld, J.H., "Effect of Surface Tension of Aqueous Methane Sulfonic Acid Solutions Upon Nucleation and Growth of Aerosol," *Atmos. Env.*, Vol. 22, No. 7, pp. 1499–1500, 1988.

Liss, D.S. and Slater, D.G., "Flux of Gases Across the Air–Sea Interface," Vol. 247, NATURE, Jan 25, 1974, pp. 181–184.

Lovelock, J.E., Maggs, R.J., and Rasmussen, R.A., "Atmospheric Dimethyl Sulphide and the Natural Sulfur Cycle," Vol. 237, NATURE, June 23, 1972, pp. 452–453.

Maum, Carlson, Coles, 1989. Sea Slick & Surface Strain. Deep Sea Research. In Press.

Saltzman, E.S., Savoie, D.L., Propero, J.M., and Zika, R.G., "Atmospheric Methane Sulfonic Acid and Non-Sea Salt Sulfate at Fanning and American Samoa," Geophy. Res. Let., Vol. 12, No. 7, pp. 437–440, July 1985.

Anon, "Methane Sulfonic Acid in the Marine Atmosphere," JGR, Vol. 88, No. C15, pp. 10,897–10,902; December 20, 1983.

Section 5

REFERENCES

1. Chylek, P., 1978: "Extinction and Liquid Water Content of Fogs and Clouds," J. of Atmos. Sci., 34, pp. 296–300, February 1978.

2. Frick, G.M., Hoppel, W.A., Fitzgerald, J.W., and Wattle, B.J., 1992: "A Cloud Chamber Study of the Effect Which Nonprecipitating Clouds Have on the Aerosol Size Distribution," NRL Report 9514, September 1992, Naval Research Laboratory, Washington, DC 20375–5000.

3. Hatakeyama, S., Izumi, K., and Akimoto, H., "Yield of SO_2 and Formation of Aerosol in the Photo-Oxidation of DMA Under Atmospheric Conditions," *Atmos. Ev.*, Vol. 19, No. 1, 1985, pp. 131–141

4. Hatakeyama, S., Okuda, M., and Akimoto, H., 1982. "Formation of Sulfur Dioxide and Methanesulfonic Acid in the Photooxidation of Dimethylsulfide in the Air," *Geophys. Res. Lett. 9*, pp. 583–586.

5. Hoppel, W.A . Fitzgerald, J.W., Frick, G.M., Larson, R.E., and Wattle, B.J., 1987: "Preliminary Investigation of the Role That DMS and Cloud Cycles Play in the Formation of the Aerosol Size Distribution," NRL Report 9032, 29 July 1987, Naval Research Laboratory, Washington, DC 20375–5000.

6. Hoppel, W.A., Fitzgerald, J.W., and Larson, R.E., 1985: "Aerosol Size Distributions in Air Masses Advecting Off the East Coast of the United States," *J. Geophys. Res.* 90, pp 2365–2379.

7. Hoppel, W.A., Frick, G.M., Fitzgerald, J.W., and Wattle, B.J., 1991: "A Cloud Chamber Study of the Effect Which Non-Precipitating Cloud Cycles Have on the Aerosol Size Distribution," Presented at 1991 Annual Meeting of the American Association for Aerosol Research, 7–11 October 1991, Traverse City, MI.

8. Rogers, C.W., 1989: "Investigation of North Atlantic Fog and Development of a Marine Fog Forecast System," Naval Environmental Prediction Research Facility, Monterey, CA 93943–5006, Contractor Report CR 89–11, July 1989.

9. Rogers, C.W., 1992: Final Report Contract No. N00014-91-C-0628, Calspan Corp., P.O. Box 400, Buffalo, NY 14225 (in preparation)

10. Yin, F., Grosjean, D., and Seinfeld, J.H., 1990: "Photooxidation of Dimethylsulfide and Dimethyldisulfide. I: Mechanism Development," *J. of Atmos. Chem.*, 11: 309–364, 1990.

11. Wu, C.H., and Niki, H., 1975: "Methods for Measuring NO_2 Photodissociation Rate. Application to Smog Chamber Studies," Environmental Science and Technology, 9, no. 1, pp. 46–52, January 1975.